Encl. B

NAS5-25481

DISTRIBUTION OF HOT STARS AND HYDROGEN IN THE LARGE MAGELLANIC CLOUD

THORNTON PAGE
NASA Johnson Space Center
Houston, Texas 77058

GEORGE R. CARRUTHERS
E. O. Hulburt Center for Space Research
Naval Research Laboratory
Washington, D.C. 20375

ABSTRACT

Imagery of the Large Magellanic Cloud, in the wavelength ranges 1050-1600 Å and 1250-1600 Å, was obtained by the S201 Far Ultraviolet Camera during the Apollo 16 mission in April 1972. These images have been reduced to absolute far-UV intensity distributions over the area of the LMC, with 3-5 arc min angular resolution.

Comparison of our far-UV measurements in the LMC with Hα and 21-cm surveys reveals that interstellar hydrogen in the LMC is often concentrated in 100-pc clouds within the 500-pc clouds detected by McGee and Milton. Furthermore, at least 25 associations of O-B stars in the LMC are outside the interstellar hydrogen clouds; four of them appear to be on the far side.

Far-UV and mid-UV spectra were obtained of stars in 12 of these associations, using the International Ultraviolet Explorer. Equivalent widths of Lα and six other lines, and relative intensities of the continuum at seven wavelengths from 1300 Å to 2900 Å, have been measured and are discussed.

Key words: Large Magellanic Cloud, interstellar hydrogen, O-B stars, far-UV

(Accepted by the Astrophysical Journal for publication 15 Sep 1981.)

I. INTRODUCTION

Far-ultraviolet imagery of the Large Magellanic Cloud was obtained with an electrographic Schmidt camera (Experiment S201) during the Apollo-16 mission, 21-23 April 1972. This imagery covered two wavelength ranges, 1050-1600 Å and 1250-1600 Å, with a limiting resolution of about 3 arc-min (Carruthers and Page, 1972). Figure 1 (Plate X) shows prints of the 3 min and 30 min exposures of the LMC in the 1250-1600 Å band. Analysis of these images was briefly discussed (together with three spectra) by Page and Carruthers (1977), and in much more detail in our S201 Far-UV Atlas of the LMC (1978) which includes absolute far-UV fluxes in the two wavelength ranges for all measurable objects in the LMC images.

Previously, Henize (1956) and Doherty, Henize, and Aller (1956) had surveyed the LMC with an objective-prism camera to obtain Hα emission intensities for all identifiable emission nebulae and emission-line stars, and McGee and Milton (1966) had surveyed the LMC in the 21-cm emission of atomic hydrogen. More recently, Davies, Elliott, and Meaburn (1976), hereafter DEM, conducted a more sensitive Hα survey and compared their observations with 21-cm and radio continuum measurements.

In this paper, we compare the results of these four surveys and discuss their significance in studies of hydrogen distributions and of far- and extreme-ultraviolet stellar flux distributions in the LMC. We also discuss recent observations of selected LMC stars made with the International Ultraviolet Explorer, and their relevance both to determinations of LMC hydrogen distributions and to the absolute and relative UV brightnesses of LMC objects.

II. DATA AND ANALYSIS

The far-ultraviolet images shown in Figure 1 (Plate X) are qualitatively useful for determining the spatial distributions of early-type stars in the LMC without confusion by images of the far more numerous cooler stars (almost all stars detected in the S201 imagery are of spectral type earlier than A2; i.e., with effective temperatures above 9000 K). It will be noted that the distribution of hot stars differs considerably from the general stellar population distribution as revealed by visual imagery; the short exposure shows the previously known OB associations and clusters, whereas the longer exposure shows the general distribution of hot stars, most of which are less luminous than those in the associations. Some structural features of interest are noted in the figure. Comparison of the UV imagery with the Hα and blue imagery of DEM (their Plates I and XXI) indicates that, for the most part, the extended nebulosities in the LMC (many of which are considerably larger than the S201 resolution limit) are not conspicuous in the far ultraviolet. This is also indicated by IUE observations of the 30 Doradus nebula (Koornneef and Mathis, 1980) and of local galactic H II regions. Thus, we presume in the following that the observed far-UV is either direct starlight or starlight scattered by dust in close proximity to the stars. As discussed in more detail later, virtually all of the Henize and DEM Hα emission regions appear to be associated with hot stars apparent in the far-UV imagery, but the converse is not true.

Quantitative analysis of the imagery is, to some extent, complicated by the effects of interstellar extinction, correction for which is particularly uncertain in the LMC because of incomplete knowledge of

E(B-V), and of the extinction vs. wavelength in the LMC. It is known from ANS and IUE observations that the LMC extinction law is considerably different from that applicable in the local regions of our galaxy and shows large variation with position in the LMC (see, for example, Nandy et al., 1980).

The procedures used for the reduction and processing of the S201 electrographic imagery have been presented in detail in our Far Ultraviolet Atlas of the Large Magellanic Cloud (Page and Carruthers, 1978) and in the Revised S201 Catalog of Far Ultraviolet Objects (Page, Carruthers, and Heckathorn, in preparation). In summary, for any identifiable image, the integrated intensity is proportional to the density volume $V = \sum(d_L - b_L)$, where d_L and b_L are the optical densities (as measured by the PDS microdensitometer used to scan the films, times 100) of each pixel in the image, and in background areas near (but outside) the image, respectively; the sum is over all pixels detectably above the adopted background. The subscript L indicates that the densities have been corrected for nonlinearities of the emulsion and microdensitometer. The density volume can then be related to ultraviolet brightness by reference to preflight calibrations of the instrument and/or comparison of observations of objects in common with other photometrically calibrated observations, such as those of OAO-2 (Code and Meade, 1979; Code, Holm, and Bottemiller, 1980). We have determined, through comparison of our preflight calibration predictions with OAO-2 measurements by Code et al. (1980) that the absolute sensitivity of the S201 camera was probably a factor of 1.5 (0.45 stellar magnitudes) less, at the time of the observations, than predicted by our preflight calibrations.

Inspection of the far-UV images gives the qualitative impression that the surface brightness of the LMC in the far-ultraviolet, relative to the visible, is very high; particularly in comparison to the local region of our galaxy and to the Andromeda Galaxy (Carruthers, Heckathorn, and Opal, 1978). Figure 2 gives a more quantitative presentation of the UV surface brightness of the LMC; shown are isodensity contours from the 10-minute 1250-1600 Å exposure. The density values have been smoothed and corrected for nonlinearity. Based on our preflight calibrations, a density above background of 0.1 corresponds to an intensity of 1.89×10^6 photons/cm^{2}sec sterad at the effective wavelength (1400 Å) of the camera. For a flat continuum extending over the camera effective passband of 250 Å, this corresponds to 7.56×10^3 photons/cm^{2}sec Å sterad (1.07×10^{-7} erg/cm^{2}sec Å sterad).

In the LMC, determination of the UV brightnesses of individual objects is difficult, because of the limited resolution of our imagery and because of the multitude of field stars against which an individual object must be observed. This makes determination of the true background which should be subtracted from the measured density, in determinations of the density volumes, very uncertain. However, contour plots such as that in Fig. 2 give useful measurements of the ultraviolet brightness distribution over the face of the LMC, which are significant to studies of the interstellar medium in the LMC (photoionization and photodissociation equilibria of many interstellar species are largely controlled by the stellar ultraviolet radiation field longward of 912 Å) and which, in conjunction with other determinations of stellar spectral type or effective temperature, provide indications of the distribution of dust extinction

over the LMC. Our measurements of the UV brightnesses of selected objects or areas are of practical utility in guiding observations with more sensitive and/or higher resolution instruments, such as the International Ultraviolet Explorer and the Space Telescope.

We obtained a measure of the total UV brightness of the LMC in the 1050-1600 Å and 1250-1600 Å ranges by summing the densities of all pixels in the LMC region of each frame, using as a background reference the uniform background densities outside, but around the borders of, the LMC image. The contributions of seven SAO stars were also subtracted. The total brightness of the LMC (based on our preflight calibrations) in the 1250-1600 Å wavelength range (λ_{eff} = 1400 Å) is 220 photons/cm^2 sec Å or $F_{1400} = 3.12 \times 10^{-9}$ ergs/cm^2 sec Å. This corresponds to a UV magnitude, in the system of Code et al. (1980), of $m_{1400} = 0.23$. In the 1050-1600 Å range (λ_{eff} = 1300 Å) the corresponding UV magnitude is $m_{1300} = 0.13$. Averaged over the apparent angular size of the LMC on our image (about 6° diameter, or 9×10^{-3} sterad) the mean surface brightness is $S_{1400} = 2.4 \times 10^4$ photons/cm^2 sec Å sterad (3.4×10^{-7} ergs/cm^2 sec Å sterad), and $S_{1300} = 2.5 \times 10^4$ photons/cm^2 sec Å sterad (3.8×10^{-7} ergs/cm^2 Å sterad). These measurements include both direct and dust-scattered starlight (we assume that nebular emission lines make a negligible contribution to the total UV brightness). As mentioned earlier, use of the OAO-2 photometry as a reference standard will increase the above intensity by a factor of 1.5. Except for a minor correction due to interstellar extinction within our galaxy in the line of sight to the LMC, this gives an indication of the local stellar radiation field, on the average, within the LMC. The average surface brightness at 1400 Å corresponds to a radiation density of $U_{1400} = \frac{4\pi}{c} S_{1400} = 1.4 \times 10^{-16}$ ergs/cm^3 Å. This may be compared with estimates of the radiation field within our own galaxy of about 10^{-16} ergs/cm^3 Å at 1400 Å (Witt and Johnson, 1973) and about half this value predicted by Henry (1977).

In our Atlas (1978) we derived a "hydrogen index" (hereafter H Ind) as the ratio of Hα flux, HA, to far-UV flux, UF (corrected for dust extinction), at over 100 places in the LMC. This index was first presented as a rough measure of the hydrogen near hot stars or star groups detected on our far-UV images. That is, if the ionizing extreme-UV ($\lambda < 912$ Å) flux is assumed roughly proportional to the far-UV flux, then the intensity of Hα emission is related to the local hydrogen density. Here, we present a revised determination of H Ind and its variation over the LMC, using a more recent determination of the LMC extinction law, allowing for extinction at Hα as well as in the UV, and utilizing additional data on the Hα brightness distribution in the LMC. Figure 3 is a contour plot of H Ind (times 100), the derivation of which is discussed in the following.

The far-UV flux values are proportional to the measured density volume, V (corrected for nonlinearities and background) divided by the exposure time, E, in minutes. As shown in our S201 Catalog of Far-UV Objects (1978), a density-volume

$$V = 0.037\ n \tag{1}$$

where n is the number of photoelectrons forming the far-UV image. Thus,

$$V/E = 6.17 \times 10^{-4}\ n \text{ per sec} \tag{2}$$

where E is the exposure time in min, and n/sec is related to the photons arriving each sec from the object. The detection efficiency (photoelectrons per photon, based on preflight calibrations) of the S201 Camera in the imaging mode averages 0.05 over the range 1050-1600 Å with the LiF corrector, and 0.04 over the range 1250-1600 Å with the CaF_2 corrector. Hence, the photon flux in these wavelengths is

$$N_L = n_L/0.05(30.0) = 1.08 \times 10^3\ (V_L/E) \text{ photons/sec cm}^2 \text{ for } 1300 \text{ Å} \pm 250 \text{ Å}, \tag{3}$$

and

$$N_C = n_C/0.04(30.0) = 1.35 \times 10^3\ (V_C/E) \text{ photons/sec cm}^2 \text{ for } 1400 \text{ Å} \pm 150 \text{ Å}, \tag{4}$$

where 30.0 cm^2 is the aperture area of the S201 camera. Since these photons each carry 1.52×10^{-11} erg and 1.42×10^{-11} erg respectively, the far-UV flux is

$$F_L = 1.64 \times 10^{-8} (V_L/E) \text{ erg sec}^{-1} \text{ cm}^{-2} \text{ and} \quad (5)$$

$$F_C = 1.92 \times 10^{-8} (V_C/E) \text{ erg sec}^{-1} \text{ cm}^{-2}. \quad (6)$$

These were corrected for interstellar extinction, based on previous estimates (Lucke 1974) of the visual reddening (RE = E(B-V)). In order to estimate reddening for all our measurements of V/E, for which specific values of RE were not available, we plotted Lucke's (1974) RE values and sketched in contour lines (see Fig. 4). Although Lucke's 81 measured values are good to $\pm$ 0.05, corresponding to $\pm$ 16 to $\pm$ 17% in corrected ultraviolet flux, UF, there is inevitably some uncertainty in the interpolated values of RE, due to small scale variations in the extinction at a given distance, and the uncertainty in distance to an object along the line of sight. The stellar associations for which Lucke determined RE may lie in front of or behind far-UV objects with nearly the same celestial coordinates. However, it is highly likely that an LH cluster and an associated Henize nebula are in close 3-dimensional proximity.

In the Far-UV Atlas, we used the "average" galactic interstellar extinction curve of Bless and Savage (1972). However, measurements with the ANS satellite (Borgman and Danks, 1977; Koornneef, 1978) in the 30 Doradus region, and with IUE (Nandy et al., 1980) there and elsewhere in the LMC indicate a higher ratio of far-UV extinction to E(B-V) in the LMC than is typical in the local region of our galaxy (see Figure 5). Using the extinction curve of Nandy et al. (1980) with $A_\lambda = 3\ E(B-V) + E(\lambda-V)$, we have, for effective wavelengths of 1300 Å (LiF corrector) and 1400 Å (CaF_2 corrector), E(1300-V)/E(B-V) = 8.97 and E(1400-V)/E(B-V) = 7.09.

Therefore, the ultraviolet fluxes corrected for reddening are

$$UF_L = F_L \, 10^{4.8\,RE} \tag{7}$$

$$UF_C = F_C \, 10^{4.0\,RE} \tag{8}$$

As expected, UF_L values for an object are generally larger than the UF_C values because of the wider bandpass and larger extinction correction at the effective wavelength of 1300 A. The scatter in the LMC extinction curve of Nandy et al. (1980) is about 0.2 mag. The extinction correction at Hα is assumed to be $A_{6563} = 2.5$ RE; hence the corrected Hα flux is $UHA = HA \cdot 10^{RE}$, approximately, where HA is the Hα flux as measured by Henize et al. (1956) in units of 10^{-4} erg/cm^{2}sec sterad. The HA values given here are often summed for several close H II regions that could not be separately resolved on our S201 photos. For instance, N180A-C means the summed flux from N180A, N180B, and N180C. In order to get a single hydrogen index representing all measurements of a given object, we averaged the values for two ILi frames with 1/2 the values for two ICa frames:

$$H\ Ind_L = UHA/UF_L \tag{9}$$

$$H\ Ind_C = UHA/UF_C \tag{10}$$

$$H\ Ind = (H\ Ind_{L1} + H\ Ind_{L2} + 1/2\ H\ Ind_{C1} + 1/2\ H\ Ind_{C2})/4 \tag{11}$$

The major errors in V/E, UF, and H Ind are due to uncertainty in background, b. As Fig. 2 shows, many of the objects measured are in regions where the background density is changing. The local background was estimated on mosaics of d, taking the first minimum in d in each of four directions from the peak density, along +x, +y, -x, and -y, and averaging these to get b. The background is high and posed the most difficulties on the 3-min ILi exposure, frame A125.

The HA values are probably good to ± 10%, although values near zero are subject to larger percentage errors. In fact, DEM, in a careful survey of a 5-hour exposure with the SRC 48-inch Schmidt camera using an interference filter with 100 Å bandpass centered on Hα and [NII], found the faint Henize H II regions much larger, and detected 100 more, most of them fainter than Henize's limit. They give no quantitative measurements of brightness, but use the steps vf (very faint), f (faint), fb (fairly bright), b (bright), and vb (very bright). We calibrated this scale against HA by assigning the numbers vf = 1, f = 2, fb = 3, b = 5, vb = 10, and multiplying by the dimensions given in arc-min. For instance, a faint (f) nebula of size 3.5' x 2' has a brightness (arc-min)^2 of 2 x 3.5 x 2 = 14. Fig. 6 is a plot of these values against HA for 64 cases where the DEM dimensions are roughly the same as Henize's. To a fairly good approximation,

$$\text{DEM brightness (arc-min)}^2 = 3\ \text{HA}. \qquad (12)$$

Using this calibration, we could fill in 227 H II regions at positions in the LMC where we had measured far-UV flux, leaving out only 19 DEM objects of the total of 356. (These positions were all searched on our mosaics.)

The surface brightness of a pure hydrogen emission nebula at Hα is proportional to the volumetric recombination rate (which in turn is proportional to the square of the hydrogen density) and to the diameter of the Strömgren sphere. For a given local hydrogen density, the diameter of the Strömgren sphere varies as the cube root of the stellar extreme ultraviolet (EUV) Lyman-continuum photon flux N_{EUV}; for a given stellar EUV flux, it is proportional to $n_H^{-2/3}$. Thus the Hα surface brightness is, in total, proportional to $N_{EUV}^{1/3}\ n_H^{4/3}$. We assume that

the diameter of the Strömgren sphere is larger than the limiting resolution (about 5 arc sec) of the Henize survey, which at the 52-kpc distance of the LMC amounts to about 1.4 pc. Using the data for typical theoretical Strömgren spheres (Spitzer, 1978, p. 110), this will be true for all stars B0 or earlier at $n_H \lesssim 60/cm^3$.

The effects of interstellar extinction, both within and near the H II regions, can be very marked, especially for regions with large n_H and correspondingly high dust densities. Although the Hα extinction is much less than the far-UV extinction, the average extinction over the projected area of the H II region is not necessarily the same as that in front of the enclosed hot stars. Measurements of radio continuum and recombination lines should help determine the extinction corrections to the Hα measurements. However, since the far-UV extinction corrections for most objects we observed are small, our assumption that the nebular Hα extinction is equal to the stellar extinction at Hα should have little effect on our results.

It is apparent that determinations of local hydrogen densities from Hα intensity measurements are very sensitive to the inferred or predicted EUV ionizing flux. Ground-based methods include determination of the stellar spectral class which, in combination with model-atmosphere predictions, can be used to infer the EUV flux. Another method is measuring directly the diameter as well as the surface brightness of the Strömgren sphere. Both of these methods have many well-known difficulties. The measurement of the stellar far-UV (1050-1600 Å) fluxes provides additional independent data which, in combination with the ground-based measurements, help to specify more accurately the stellar effective temperature, and

thereby better infer the EUV flux. This, in turn, can yield more accurate estimates of local hydrogen density. Measurements of the exciting stars in the far ultraviolet, although not directly indicative of the Lyman continuum, are much more useful than measurements in visible wavelengths because they are much closer to the Lyman continuum. Also, by being near the peak continuum of early-type stars, far-UV is much more sensitive to small differences in effective temperature. Figure 7 shows model atmosphere stellar flux distributions computed by Kurucz, Peytremann, and Avrett (1974), normalized to 5500 Å.

In addition, far-UV measurements, in combination with ground-based measurements, can be used to estimate the effects of interstellar extinction with much better accuracy than can measurements in the ground-accessible wavelengths alone, because extinction (particularly in the LMC) is so much larger below 1600 Å. Ideally, it would be better still to also have measurements in the "extinction bump" near 2200 Å (see Bless and Savage (1972), Savage (1975), Nandy et al. (1980)). Assuming that interstellar extinction can be determined from a combination of ground-based and UV data Figure 7 shows that measurements of the far-UV/visible ratio can be used to infer the effective temperature, and hence the EUV/visible ratio. This ratio is, however, increasing considerably faster with effective temperature than is the far-UV/visible ratio in the temperature range of interest, and hence accurate measurements are necessary. Figure 8 shows ratios of integrated EUV/visible, and far-UV (ILi spectral range)/visible, where the visible photon flux is integrated over the range 5000-6000 Å. Also shown are the ratios of EUV to far-UV photon flux, and of photon fluxes in the ILi and ICa spectral ranges. (EUV is labelled LyC for Lyman continuum.)

The Hydrogen Index, as derived from our measurements, gives only qualitative indications of stellar effective temperature and local hydrogen densities. This is because the limited angular resolution of the S201 camera prevents, in most cases, the attribution of a given UF value to a single star, and hence comparison of the UV flux with ground-based measurements of the same star. In a rich cluster or association, therefore, a given UF could be produced by a single O star with effective temperature of 40,000 K, or by a cluster of B stars with effective temperatures near 20,000 K, but the Lyman continuum flux would be much larger in the former case. However, the Hydrogen Index is a quantitatively useful criterion for analysis of higher-resolution measurements, in which single stars can be isolated (e.g., with the IUE satellite), and in which flux distributions and effective temperatures can be determined individually for all of the UV-bright stars associated with a given H II region. In the following, we present a qualitative comparison of our Hydrogen Index measurements with 21-cm observations of atomic hydrogen, and discuss the potential of IUE observations for refinements of both interstellar hydrogen and effective temperature measurements.

III. COMPARISON WITH 21-CM OBSERVATIONS

More direct methods of estimating interstellar hydrogen concentrations include measuring the Lyman-α interstellar absorption line in the spectra of hot LMC stars, and mapping the 21-cm radio emission across the LMC. The Lα measurements are to be preferred over 21-cm measurements for several reasons (Carruthers, 1970, and Jenkins, 1970), such as better spatial resolution, discrimination against hydrogen beyond the star of

interest, and freedom from the effects of spin temperature, concentration, etc. Nevertheless, since 21-cm measurements were available and Lα measurements (until recently, with the advent of the IUE satellite) were not, we decided to compare our Hydrogen Index values first with radio measurements of hydrogen in the IMC.

We compared Fig. 3 with the 21-cm survey by McGee and Milton (1966). Their measurements of brightness temperature, T_b, are presented in three different contour plots, showing values for radial velocities near 300, 273, and 243 km/sec. We combined these, taking the largest T_b at each location, and this combined 21-cm flux is presented in Fig. 9, where contours of 20, 30, 40, and 50 flux units are shown. (1 flux unit = 1.76 K in T_b.) Although there are some similarities between Figs. 3 and 9, there are some notable differences, where peaks in H Ind occur at low values of the 21-cm flux. McGee and Milton noted one of these in comparing their hydrogen clouds with Karl Henize's (1956) H II regions; the nebula N55 at $5^h32^m.3 - 66°28'$ has no strong 21-cm flux near it.

There are at least 30 other similar cases in Tables 1 and 2. Moreover, we find about 50 regions of high UF in the H I clouds with little or no Hα emission, and therefore zero or low H Ind, as shown in Table 3. Tables 1, 2, and 3 have 17 columns, the first 16 being the same in all three tables.

Col. 1 is the Davies-Elliott-Meaburn (1976) or Henize (1956) number, mostly blank in Table 3. For the Henize (N) numbers, N77A-E means N77A + N77B + N77C + N77D + N77E; N79CE means N79C + N79E; N8,A means N8 + N8A. A blank means no measured Hα flux.

Col. 2 lists the 1950 coordinates of the area measured on S201 frames A124, A125, A129, and A130.

Col. 3 is the Lucke-Hodge (1970) number of a stellar association in the LMC.

Col. 4 is the NGC number of a star cluster in the LMC.

Col. 5 lists the north-south and east-west dimensions of the measured area in arc-min.

Col. 6 is the Hα flux in units of 10^{-4} erg sec^{-1} cm^{-2} $sterad^{-1}$ summed for all the nebulas entered under N No.

Col. 7 is the unreddened flux (UF) measured on ILi frames A124 and A125, averaged.

Col. 8 is 100 times the ILi Hydrogen Index calculated from cols. 6 and 7.

Col. 9 is the unreddened flux (UF) measured on ICa frames A129 and A130, averaged.

Col. 10 is 100 times the ICa Hydrogen Index calculated from cols. 6 and 9.

Col. 11 is 100 times the mean of ILi H Ind and 1/2 ICa H Ind, our best estimate of the Hydrogen Index for the H II region(s) listed in col. 1.

Col. 12 is the McGee-Milton (1966) H I-cloud number.

Col. 13 lists the north-south and east-west diameters of the cloud in arc-min.

Col. 14 is the 21-cm flux at the location of the measured area given in col. 2, in units of 1.76 K in T_b.

Col. 15 lists the 1950 coordinates of the H I-cloud center.

Col. 16 lists the distance in arc-min and the approximate direction from cloud center to the measured area given in col. 2.

Col. 17 in Tables 1 and 2 gives the MC catalog (McGee et al. 1972) number of a radio source coincident with the H II region, and the letters

SNR for supernova remnant identified by its non-thermal radio spectrum.

Col. 17 in Table 3 is the reddening (RE), or color excess, interpolated from Lucke's (1974) measurements.

In five regions of the LMC, Table 1 shows both high Hydrogen Index and high 21-cm flux. These regions are centered at:

$4^h{}^m.8-69^o:20'$	involving N77,79,81,	mean H Ind = 69,	and H I cloud L34,	21-cm flux = 38
4:58.6-66:18	N11,12,13,	64	L2	42
5:14.3-69:25	N112,114	127?	L39,40,43	30
5:29.1-71:15	N199,200,206	47	L46,47	30
5:34.0-67:39	N56,57,59	100	L13,14	35

These regions are evidently in the H'I clouds and well populated with clusters of O-B stars, from LH2 and NGC 1727 in L34 to LH76 and NGC 2014 in L13 and L14. The mean H Ind x 100 is about 2.3 times the 21-cm flux.

Five other H Ind maxima in Table 1, and all those in Table 2, total 25 H II regions outside of the H I clouds, where the unreddened far-UV flux, UF, is strong enough to ionize the hydrogen where the 21-cm flux is only 10 to 20. This indicates small H I concentrations along the line of sight. The mean H Ind x 100 is about 4.75 times the 21-cm flux.

The ratio of the H II-region area to the H I-cloud area in Table 1 ranges from less than 1% to 52% for L14 and 59% for L2, with some indication of a correlation with the 21-cm flux, which ranges from 15 to 50 units. Eleven H I clouds have more than 15% of their area covered with H II regions, and the average for all listed in Table 1 is 12%.

In Table 3 there are 38 regions in the H I clouds where there is high UF from clusters of O-B stars and little or no Hα flux, leading to zero or low H Ind. These clusters of O-B stars must therefore be in front of or behind the H I clouds. From the RE values -- E(B-V) -- in Table 3, it seems likely that four clusters are <u>behind</u> the H I clouds:

NGC 1734 (and D14,16) at $4^h53^m.3-68^o56'$, behind L23

LH85,89 and NGC 2042 at 5:36.2-68:55, behind L32

and at 5:36.5-68:57, behind L32

and NGC 2100 at 5:42.4-69:13, behind L32.

Most of the others are probably in front of the H I clouds. The sizes of these strong UF areas are smaller than the H II regions in Table 1. They range from less than 1% to 20% of the H I-cloud area in L25, and 28% in L10; the average of all listed in Table 3 is 6%. It is unlikely that these are foreground stars, since SAO stars have been omitted from the list.

We conclude that the <u>local</u> hydrogen density near the objects listed in Table 3 is too low (below $\approx 2/cm^3$) to produce a measurable Hα nebula, although the total <u>column</u> densities are large. This indicates that the Hydrogen-Index method may provide useful measurements of <u>local</u> hydrogen density, which can be compared with the <u>column</u> densities observed by other methods, such as 21-cm emission and Lα absorption.

IV. IUE OBSERVATIONS

Extensive measurements have been made of the column densities of interstellar atomic hydrogen in the lines of sight to relatively nearby galactic stars using the OAO-2 far ultraviolet spectrometer (Savage and

Jenkins, 1972; Jenkins and Savage, 1974) and with the much higher-resolution instrument on the OAO-3 (Copernicus) spacecraft (Bohlin, 1975; Bohlin, Savage, and Drake, 1978). However, both of these instruments were limited to relatively bright stars, and so were unable to obtain observations in the Large Magellanic Cloud.

The International Ultraviolet Explorer (IUE) satellite, however, can observe much fainter objects than its predecessors, allowing observations of interstellar H in the directions of O and early B stars in the LMC at low dispersion (7 Å resolution); at longer wavelengths, a few objects have been observed at high dispersion (0.1 Å resolution). de Boer, Koornneef, and Savage (1980) observed HD 38282 (R144) and HD 38268 (R136), obtaining H column densities of $1.9 \times 10^{21}/cm^2$ and $7 \times 10^{21}/cm^2$, respectively. Subtraction of an estimated local galactic column density of $7 \times 10^{20}/cm^2$ yielded 1.2 and $6.3 \times 10^{21}/cm^2$, respectively, for the LMC contribution to the observed column densities.

In early 1979 (27 January - 3 February) one of us (TP) obtained IUE observations of a number of LMC stars, in low dispersion mode, which were associated with bright objects in the S201 UV imagery. These spectra were taken for the purpose of measuring the hydrogen column densities (from the Lα absorption features) and for obtaining measures of the absolute flux distributions and spectral types for correlation with the direct imagery. The procedure used was to select the brightest star (as seen by the IUE slit jaw camera) associated with a selected LH association and/or Henize nebula. In some cases, this star turned out to be of late spectral type and yielded an underexposed spectrum. (The coordinates

we had available were not sufficiently accurate to allow us to select individual stars for which ground-based photometry and spectral classification were available.)

Table 4 lists 30 IUE spectra of 14 different stars in 12 of the associations, including one from Table 1 and three each from Tables 2 and 3. In one set of two exposures, two stars were in the slit (large aperture, 23.2 x 10.4 arcsec), and two separate spectra of LH 74 = NGC 2015 stars were obtained, somewhat underexposed. Column 1 of Table 4 lists the Henize (1956) N number or the Davies-Elliott-Meaburn (1976) D number, and the the Lucke-Hodge (1970) Association or NGC number. In some cases, there is no Hα nebula. Column 2 lists our Hydrogen Index (x 100); Column 3 the McGee-Milton (1966) 21-cm flux; Column 4 is IUE far-UV (SWP) image number; Column 5 the exposure in minutes; Columns 6 to 8 are the continuum fluxes at 1300, 1400, and 1500 Å relative to that at 1925 Å; Columns 9 to 14 are rough equivalent widths of Lα, Si III (1300 A), C II (1335 A), Si IV (1394, 1403 A), C IV (1550 A), and the feature at 1720 A. Column 15 is the reddening (RE) = E(B-V), interpolated from the values of Lucke (1974); Column 16 is the mid-UV (LWR) image number; Column 17 the exposure in minutes; Columns 18 to 20 are the continuum fluxes at 2325, 2675, and 2900 A, relative to that at 1925 A; Column 21 is the equivalent width of Mg II (2804 A); and Column 22 is the spectral type estimated by Karl Henize (private communication, 1980) from the Si IV to C IV line ratios, or by us from a comparison with Copernicus U2 spectra of standard stars degraded to 6.2 A resolution comparable to that of the IUE low-dispersion spectrograph.

All of the measurements were made from the IUE Calcomp plots of the net spectrum flux number *vs* wavelength after correction for distortion, nonlinearity, and initial IUE calibration error. The equivalent widths are products of the line width at half depth and the central depth as percentage of continuum. Lα has been corrected for geocoronal emission by using the Lα emission in the small-aperture spectrum, as shown in Fig. 10. The ratio of area of the large aperture to that of the small aperture (3.2-arc-sec circle) was determined (Penston, private communication) to be 31.1 $\pm$ 1.9, and the ratio of widths parallel to dispersion is 4.0. The small-aperture profile on the Calcomp plot is always a triangle of base *w* and height *P*. This was scaled up to a triangle of base 4w and height 31.1 P/4 = 7.75 P centered at 1215 Å (the apparent wavelength of Lα at the LMC radial velocity), and subtracted from the large-aperture plot. (This scaling factor was confirmed by IUE spectra where only geocoronal Lα was present in both apertures.) The remaining Lα, the stellar absorption line (or no line, or emission line) was then measured for equivalent width in the same way as the other stellar lines. In two cases, the stellar contribution came out as an emission line (LH 88 and LH 89 in Table 4).

The errors in measuring these line profiles are rather large, but the potential for improvement is limited by the low spectral resolution and photometric accuracy of the raw data. For stars of spectral type later than B2-B3, the width of the stellar Lα absorption is comparable to or greater than that of the interstellar line, preventing determinations of the interstellar H column density by this method. However, for the

hotter stars in which the stellar contribution is negligible, the hydrogen column density can be estimated from the relationship

$$N(H\ I) = 1.37 \times 10^{19} (W_{1216})^2 \qquad (13)$$

where $W_{1216} = 1.476$ FWHM (York, 1976). These column densities, also listed in Table 4, are subject to large uncertainties due to errors in correcting for geocoronal Lα emission (as mentioned above) and for nearby stellar features, such as blueshifted N V absorption and Si III (1200 Å) absorption. Two examples in Table 4 where the Lα equivalent widths are clearly in excess of the stellar component (based on the spectral type derived from other lines), are LH 111 and LH 64.

Spectral types were estimated, and flux distributions measured, for the observed stars for comparison with the S201 imagery, and for refining our Hydrogen Index measures. The spectral types in col. 22 of Table 4 are estimates by K. Henize based on the equivalent widths of Si III (1300 Å), Si IV (1394, 1403 Å), and C IV (1550 Å) and by one of us (TP) using Si III, C II (1335 Å), and Si IV for types later than B3. Surprisingly, there is only one supergiant in this sample of bright early-type stars in the LMC. The deviations are about two spectral classes in the B types. As indicated in Table 4, the luminosity classes are also approximate.

The continuum fluxes (relative to 1925 Å) were determined using the latest IUE calibration (Bohlin et al., 1980). These are listed in Table 4 (and plotted in Fig. 11). The continuum intensity generally decreases from 1300 to 2900 Å, as expected for early-type stars. For comparison with the model atmosphere predictions of Kurucz et al. (1974), Table 5 was

generated using the reddening law of Nandy et al. (1980), Fig. 5, and the RE values of Lucke (1974), see Fig. 4. Table 6 gives the best matches of the observed flux distributions to the reddened model predictions. It is seen that, in several cases, the observed flux distributions indicate considerably higher effective temperatures than do the ultraviolet line ratios. This could be due to (a) hotter but less luminous stars which contribute to the continuum more than to the spectral line absorptions, (b) overestimation of the local reddening, and (c) measurement errors in the line and/or continuum determinations.

All in all, these IUE measurements tend to confirm our conclusions from the S201 far-UV measurements, including spectrographic results (Carruthers and Page, 1977) but do not add very much. Because of an unexpected early assignment of IUE observing time, we could not select individual stars classified by Lucke and Hodge (1970), Ardeberg et al. (1972), and Walborn (1977). Also, we were not able to systematically observe all of the UV-bright stars in specific associations associated with specific Hα emission regions. However, further analysis of our present observations, and follow-on observations with IUE, will allow better correlation of our results with previous ground-based observations as well as with the S201 measurements.

V. CONCLUSIONS

The far-ultraviolet brightness distribution over the face of the Large Magellanic Cloud has been determined from calibrated electrographic imagery in the 1050-1600 and 1250-1600 Å ranges. Far-UV fluxes for individual hot-star groupings in the LMC have been compared with Hα measurements (Henize, 1956; Doherty et al., 1956; Davies et al., 1976)

and with the McGee and Milton (1966) 21-cm survey. These comparisons indicate that large clouds of interstellar hydrogen contain smaller concentrations revealed by Hα emission, and other clear regions where hot O-B stars excite no H II regions (undetectable Hα). Four of these associations probably lie behind the large interstellar clouds. Alternatively, these clouds may be very diffuse and extended in the line of sight. Six other peaks in far-UV flux not previously catalogued are also indicated. Initial exploratory investigations of H Lα absorption using the IUE satellite tend to confirm these results.

We recommend further IUE measurements of Lα absorption and dust extinction in the spectra of hot stars observed by Lucke and Hodge (1970) in the IMC associations listed in Tables 1, 2, and 3, as well as radio continuum and recombination-line measurements, and higher-resolution 21-cm measurements in these regions. More detailed IUE measurements of flux distributions, and spectral type/effective temperature determinations, for all stars associated with particular Hα emission regions would allow for our Hydrogen Index measure to be placed on a more quantitative basis. High-resolution observations at Lα would be highly desirable; although marginal with IUE these should be readily possible with Space Telescope.

Ground-based photometry, with angular resolution equal to that of the S201 Camera (3 arc-min) in areas around the UF peaks we observed, would be particularly useful, as well as more detailed photometric measures of the individual stars. The photometers should utilize narrow-band interference filters, so as to isolate emission-line-free segments of continuum for stellar photometry. In addition, measurements of nebular emissions such as Hα, but with higher photometric accuracy than in previous work are

needed. Higher angular resolution 21-cm measurements, if possible equal to or better than the 3 arc min resolution of S201, would be very useful.

Part of this research was supported by NASA Grant NASW-3023. We thank Dr. Karl Henize for useful discussions, and the IUE Observatory Staff for their support of our observations. The IUE observations and data reduction were supported by NASA Grant NAS5-25481.

Table 1. Regions of High Hydrogen Index in 21-cm Clouds

DEM or N No.	RA(1950)DEC	LH No.	NGC No.	ΔδxΔα Size†	HA	L-Filter UF	L-Filter HInd.	C-Filter UF	C-Filter HInd.	100x Mean HInd.	Cloud No.‡	ΔδxΔα Size†	Fl.	RA(1950)DEC	Dist. to Neb.*	MC No.
	h m o													h m o		
N77A-E*	4:49.7-69:17'	--	--	8.4x 7.2	3.4	158	108	104	150	92	L34	42x50	45	4:50.1-69:18'	3W	10
N79CE*	4:52.5-69:25	2	1727	6.0x 6.0	58.0	245	44	99	74	40	|		35		19E	
N81AB	4:53.1-69:18	--	--	3.6x 3.6	11.6	48?	22?	10	206	76?	|		35		22E	
N76	4:49.2-68:29	--	--	3.6x 4.8	4.5	12	112	0	--	112	L21Ed	32x58	20	4:50.7-68:13	19S	
N8,A*	4:53.1-68:08	--	--	4.8x 3.6	23.1	31	93	9	276	115	|		20		18E	
N5	4:52.6-67:22	3	--	6.0x 6.0	35.2	70	67	26	182	79	L1	44x20	15	4:51.4-67:06	18SE	
N7	4:53.5-67:28	--	--	3.6x 3.6	3.2	16	75	0	--	75?	| Ed		15		27SE	
N11,A-L*	4:56.6-66:30	9-14	1760-73	26.2x23.9	1874.0	18772	15	665	30	15	L2	36x43	30	4:58.2-66:24	13SW	18
N11BC*	4:57.2-66:30	9,13	1760-69	7.2x 8.4	355.0	952	54	355	146	65	|		30		9S	
N12,A	4:58.6-66:16	--	--	7.2x 6.0	26.8	73	51	33	110	53	|		50		9W	
N13	5:00.1-66:09	--	--	4.8x 4.8	4.0	12?	45?	3	180	75	| Ed		45		19NE	
N80	4:54.3-68:27	--	--	3.6x 3.6	9.2	63	24	18	81	32	L23	46x34	25	4:54.3-68:32	6N	
N84	4:55.7-68:31	--	--	4.8x 4.8	10.8	212	9	10	197	52	|		25		6E	
D56	5:03.0-66:44	--	--	3.6x 4.2	47.0	--	--	68	102	51	L4	46x38	20	5:05.0-66:54	18NW	
N20	5:05.2-66:59	--	--	3.6x 4.8	4.0	33	18	3	188	56	|		25		5S	21
D72	5:05.4-65:42	--	--	4.8x 4.8	25.0	115	31	65	57	30	L3 Ed	25x34	30	5:04.0-65:55	16NE	
N21	5:04.9-67:38	22	--	4.8x 6.0	11.8	34	43	13	109	49	L37Ed	29x30	10	5:02.4-67:53	24NE	
N17,AB	5:03.8-67:23	19	--	3.6x 4.8	8.9	13	144	30	43	83?	| Ed		10		32N	
N21	5:04.9-67:38	22	--	4.8x 6.0	11.8	34	43	13	109	49	L38	24x40	10	5:04.5-67:26	12S	
N17,AB	5:03.8-67:23	19	--	3.6x 4.8	8.9	13	144	30	43	83?	|		10		9NW	
N103AB	5:09.2-68:50	--	--	8.4x 6.0	104.3	846	18	451	34	17	L39Ed	38x32	18	5:11.3-69:05	21NW	SNR
N112	5:13.7-69:15	--	--	3.6x 3.6	3.3	5?	95?	0	--	95?	| Ed		30		20E	
N114,A	5:14.9-69:34	39	--	10.7x 8.4	159.1	199	117	88	406?	160?	| Ed		22		39SE	
N108	5:10.8-69:31	--	--	3.6x 3.6	1.6	11?	21?	0	--	20?	L40	25x38	20	5:12.4-69:34	12W	
N112	5:13.7-69:15	--	--	3.6x 3.6	3.3	5?	95?	0	--	95?	| Ed		30		21NE	
N114A	5:14.9-69:34	39	--	10.7x 8.4	159.1	199	117	88	406?	160?	|		22		18E	
N193A-E*	5:13.0-70:28	--	--	3.6x 3.6	4.8	25	32	5	158	54	L41	36x30	20	5:12.6-70:32	5E	
D119	5:16.0-71:38	--	--	2.5x 2.5	6.0	44	21	7	180	55?	| Ed		15		25E	
N30,A-D	5:13.8-67:28	34-38	1869,71	11.9x 9.5	90.7	500	23	217	56	26	L6	29x36	22	5:13.5-67:36	8N	
N33	5:16.9-67:23	--	--	3.6x 3.6	10.5	37?	38	0	--	38?	| Ed		15		28NE	
N40	5:21.5-65:30	43	1923	3.6x 3.6	5.5	87?	10?	5	166	59?	L10	24x24	15	5:22.6-65:38	11NW	

Table 1. High HInd. (Cont. p. 2)

DEM or N No.	RA(1950)DEC	LH No.	NGC No.	ΔδxΔα Size†	HA	L-Filter UF	L-Filter HInd.	C-Filter UF	C-Filter HInd.	100x Mean HInd.	Cloud No.#	ΔδxΔα Size†	Fl.	RA(1950)DEC	Dist. to [illegible]	MC
N36	5:18.0-67:57	--	--	3.6x 3.6	1.0	14	14	0	--	14	L7 Ed	37x27	20	5:16.5-68:11	18NE	
N36	5:18.0-67:57	--	--	3.6x 3.6	1.0	14	14	0	--	14	L9 Ed	38x43	20	5:21.7-68:01	27W	
N44BCF*	5:21.8-67:58	47	1929-36	7.2x 8.4	84.2	4370	5	945	14	6	L		40		3N	32SW
N37	5:20.3-66:56	--	--	4.8x 6.0	12.2	29	90	6	268	112	L8	30x36	20	5:21.7-66:48	13SW	
N38	5:20.6-66:50	--	--	3.6x 3.6	7.6	8	130	2?	450?	162?			30		8SW	
N45,A	5:22.8-66:44	--	--	3.6x 3.6	5.0	5	161	0	--	161			28		9E	
N49A-C	5:25.7-66:19	52	1948	7.2x 3.6	20.3	36	66	22	109	61	L12	43x23	35	5:26.1-66:15	5SW	40SW
N49	5:26.0-66:08	53	--	3.6x 3.6	13.2	6	291	1?1	551?	452?	L		40		7N	43yr
N199,200	5:24.0-71:23	50	--	15.5x 9.5	121.0	487	38	133	158	58	L46	57x51	20	5:25.9-71:36	19NW	
N144,AB	5:26.9-68:52	58	1962-66	10.7x10.7	475.4	2732	22	949	63	27	L29Ed	43x36	15	5:23.5-69:01	27NE	47SW
N206,A-D*	5:31.3-71:07	66,69	--	17.9x20.2	1395.3	7452	28	2201	94	37	L47	30x50	35	5:31.3-71:13	6N	54
N148B-E*	5:32.0-68:34	71	--	6.0x 4.8	21.4	150	25	91	38	22	L31	40x32	40	5:32.4-68:27	8S	56
N148I*	5:32.1-68:42	73	--	6.0x 6.0	19.2	200?	10?	0	--	10?			30		15S	55SW
N148A*	5:33.0-68:25	--	--	2.4x 2.4	1.1	27	6	6	29	11			40		3E	56
N57,A-E*	5:32.5-67:43	76	2014	13.1x13.1	711.6	2483	36	882	100	43	L13	34x30	35	5:32.1-67:50	8N	57SW
N57,A-E*	5:32.5-67:43	76	2014	13.1x13.1	711.6	2483	36	882	100	43	L14Ed	28x25	35	5:35.9-67:38	25SW	SMC
N56,59A-C	5:35.6-67:35	82,88	2029-40	9.5x11.9	543.2	466	152	209	335	160	L		35		4NW	64
N62AB	5:34.5-66:16	--	--	6.0x 4.8	41.9	59	100	25	202	101	L15Ed	34x25	10	5:37.7-66:23	24NW	62
N63,A	5:35.6-66:01	83	2030	8.4x 7.2	101.8	280	45	132	95	46	Ed		10		20NW	63SW
N64A-C*	5:37.1-66:21	95	--	7.2x 8.4	91.3	125	92	47	227	103	L		25		2N	
N213,A*	5:39.0-70:42	--	--	4.8x 6.0	48.7	495	20	87	112	38	L49	57x38	30	5:40.4-70:11	23S	
N213,A*	5:39.0-70:42	--	--	4.8x 6.0	48.7	495	20	87	112	38	L50	72x57	30	5:40.4-71:04	23N	
N214CFGH*	5:42.3-71:20	107,110	2103	6.0x 6.0	93.9	602	28	185	90	37			35		22SE	80
N214,A-H*	5:41.6-71:16	107	2103	16.7x11.9	179.1	2527	13	540	59	21	L		35		17SE	
N160,A-F*	5:40.8-69:38	103	2077-86	15.5x14.3	771.9	14721	11	4865	32	13	L48	46x27	35	5:39.7-69:44	11N	76SW
N159,A-L*	5:40.4-69:46	105	2078-84	7.2x 7.2	102.6	630	33	0	--	33	L		40		5E	77
N169A-C	5:46.7-69:34	--	--	3.6x 3.6	6.8	19	67	0	--	67	L51	32x30	45	5:46.5-69:27	7S	SMC

Table 1. High HInd. (Concld. p. 3)

DEM or N No.	RA(1950)DEC	LH No.	NGC No.	Δδ×Δα Size†	HA	L-Filter UF	L-Filter HInd.	C-Filter UF	C-Filter HInd.	100× Mean HInd.	Cloud No.#	Δδ×Δα Size†	Fl.	RA(1950)DEC	Dist. to Neb.†	MC No.
N214CFGH	5:42.3-71:20	107,110	2103	6.0x 6.0	93.9	602	28	185	90	37	L33Ed	32x30	35	5:43.4-71:07	15SW	80
N214,A-H	5:41.6-71:16	107	2103	16.7x11.9	179.1	2527	13	540	59	21	⌊ Ed		35		16SW	
N163	5:43.6-69:46	--	--	6.0x 6.0	63.0	522	28	52	247	76?	L52Ed	48x30	40	5:47.2-69:44	26W	84
N180,A-C	5:49.5-70:05	117,118	2122	16.7x13.1	337.8	14872	5	3894	18	7	⌊ Ed		30		28SE	{90SW 91
N164	5:42.9-69:05	113	--	7.2x 7.2	123.0	562	50	145	152	63	L32Ed	36x53	40	5:40.0-68:53	25SE	79,8
N165	5:43.2-68:58	109	2093	3.6x 3.6	12.7	79	29	25	94	38	⌊ Ed		35		34E	85
N169A-C	5:46.7-69:34	--	--	3.6x 3.6	6.8	19	67	0	--	67	L17	38x46	45	5:48.1-69:31	10W	89SW

Footnotes to Table 1:

* Nebula with measured radial velocity approximately the same as that of the HI cloud.

† North-south and east-west diameters given in arc-min. Distance in arc-min and approximate direction from cloud center to nebula.

\# Ed following Cloud No. indicates that the HII region is near the edge of the HI cloud.

Table 2. HII Regions Outside 21-cm Clouds

DEM or N No.	RA(1950)DEC	LH No.	NGC No.	ΔδxΔα Size	HA	L-Filter UF	L-Filter HInd.	C-Filter UF	C-Filter HInd.	100x Mean HInd.	Nearest Cloud No.	ΔδxΔα Size	Fl.	RA(1950)DEC	Dist. to Neb.	MC No.
	h m o													h m o		
N2	4:43.7-68:04'	--	--	2.4x 2.4	3.4	28	15	2	200	7?	L21	32x58	10?	4:50.7-68:13'	51W	
N10	4:55.6-66:00	--	--	3.0x 3.0	31.0	--	--	11	357	178?	L2	36x43	10	4:58.2-66:24	30NW	
N185	4:54.2-70:05	--	--	9.5x 9.5	60.6	293	30	118	67	32	L36	30x44	10	4:58.6-70:18	35NW	
N94A-C	4:57.0-69:33	8	--	6.0x 6.0	20.9	147	19	30	110	38	L34	42x50	15	4:50.1-69:18	52E	
D54	5:02.5-69:38	--	--	3x 3	4.0	322	2	4	192	64	L24	28x57	10	4:58.6-68:58	45SE	
N191AB	5:05.2-70:58	23	--	3.6x 3.6	8.4	49	24	23	50	25	L42	30x34	10	5:13.5-71:10	61W	
N100	5:07.5-68:37	--	--	4.8x 6.0	5.5	91	9	7	111	32?	L25	27x36	18	5:03.6-68:35	29E	
N104AB	5:09.7-68:33	--	--	4.8x 6.0	11.4	91	17	31	52	22	L7	38x27	20	5:16.5-68:11	53W	
D89	5:09.7-67:57	--	--	10x 8	133.	--	--	~~164~~	~~71~~	~~36~~?	L6	29x37	15	5:13.5-67:36	33SW	
N127AB,9	5:22.0-69:43	--	--	3.6x 3.6	18.7	8?	315?	0	--	300?	L28	30x36	15	5:19.4-70:10	31NE	
N132A-J	5:24.1-69:40	--	--	6.0x 8.4	11.4	240	8	147	11	6	L28	30x36	10?	5:19.4-70:10	45NE	39SN
N142	5:25.9-69:28	46	--	6.0x 4.8	10.4	83	17	18	78	28	L29	43x36	10?	5:23.5-69:01	32SE	
N51BE	5:26.7-67:41	55	--	10.7x11.9	315.9	326	125	198	205	114	L9	38x43	25?	5:21.7-68:01	41NE	
N204	5:28.0-70:36	62	--	6.0x 6.0	64.0	369	26	126	74	31	L47	30x50	10?	5:31.3-71:13	44NW	
N149AB	5:33.3-69:48	--	--	2.4x 2.4	1.9	14	25	0	--	25	L48	46x27	10?	5:40 -69:49	48W	
N55,A	5:32.3-66:28	72	--	9.5x 7.2	173.3	284	72	189	115	65	L15	34x25	10	5:37.7-66:23	41W	
D286?	5:40.9-67:04	--	--	2.4x 2.4	6.0	17	51	4	217	80?	L14	28x35	10?	5:35.9-67:38	50NE	
N160,A-F	5:40.8-69:38	103	2077-86	15.5x14.3	771.9	1472	11	4865	32	13	L51	32x30	35	5:46.5-69:27	43W	
N164	5:42.9-69:05	113	--	7.2x 7.2	123.0	562	50	145	152	63	L51	⌐	40	⌊ -- ⌊	34NW	79,82
N165	5:43.2-68:58	109	2093	3.6x 3.6	12.7	79	29	25	94	38	L51	⌊	35		38NW	85
N70	5:43.5-67:51	114	--	9.5x 9.5	240.0	463	72	238	133	69	L14	28x35	20	5:35.9-67:38	56E	
N71	5:43.9-67:27	--	--	3.6x 3.6	3.4	10	42	2	214	75	L14	28x35	18	5:35.9-67:38	59E	
N74,AB	5:45.8-67:09	116	--	7.2x15.5	93.3	355	29	246	46	26	L16	44x43	15?	5:45.6-66:19	50S	
N75AB	5:56.2-68:12	122	--	7.2x 8.4	38.3	205	24	77	63	27	L18	46x36	25	5:49.3-68:55	66NE	
D328	5:52.5-68:14	121	--	15.5x 6.0	14.0	366	6	150	12	6	L18	46x36	10?	5:49.3-68:55	47NE	92SNR

Table 3. Regions of High UF, Zero or Low HInd. in 21-cm Clouds

DEM or N No.	RA(1950)DEC	LH No.	NGC No.	ΔδxΔα Size	HA	L-Filter UF	L-Filter HInd.	C-Filter UF	C-Filter HInd.	100x Mean HInd.	Cloud No.	ΔδxΔα Size	Fl.	RA(1950)DEC	Dist. to UF	RE
	h m o '													h m o '		
--	4:50.2-69:06	--	1698?	4.8x 3.8	0	26	0	29	0	0	L34	42x50	40	4:50.1-69:18	12N	.16
D14,16	4:53.3-68:56	--	1734?	10.7x 6.6	7.5	491	3	1310	1	2	L23Ed	46x34	28	4:54.9-68:32	26SW	.25
--	4:54.4-68:35	--	--	2.4x 2.4	0	95	0	--	0	0	|		25		5SW	.20
--	4:55.5-68:15	--	1755	6.2x 6.6	0	370	0	177	0	0	|		20		17N	.17
D21	4:54.1-70:40	--	1754?	5.0x 5.4	2.8	230	3	98	5	2	L35Ed	38x59	22	4:50.1-71:00	35NE	.14
--	4:55.6-70:56	--	--	3.8x 4.5	0	72	0	39	0	0	| Ed		20		40E	.13
--	4:55.0-70:18	--	1766?	2.4x 2.5	0	70	0	9	0	0	L36Ed	30x44	10	4:58.5-70:19	25W	.15
--	4:55.3-70:26	--	1754?	4.2x 4.8	0	225	0	51	0	0	| Ed		12		24W	.15
--	4:56.2-70:17	--	1766	2.5x 2.5	0	120	0	11	0	0	|		10		17W	.16
--	4:57.5-66:28	13	1769	6.0x 6.0	0	91	0	0	--	0	L2	36x43	40	4:58.2-66:24	6SW	.15
D62	5:04.0-69:05	17	--	4.8x 3.6	1.3	87	2	26	8	3	L24Ed	32x57	19		39E	.16
--	5:03.9-69:03	16-22	-	8.5x 8.5*	0	582	0	200	0	0	| Ed		20		38E	.16
--	5:01.6-67:24	--	--	2.4x 2.4	0	70	0	8	0	0	L38Ed	24x40	10	5:04.5-67:26	21W	.16
--	5:04.4-68:29	--	--	4.6x 4.2	0	167	0	47	0	0	L26	46x26	18		16SW	.15
--	5:06.9-68:28	--	1838?	14.3x 9.4	0	2095	0	1472	0	0	|		18		18SE	.16
--	5:04.4-68:29	--	--	4.6x 4.2	0	167	0	47	0	0	L25	27x36	18	5:03.6-68:35	8NE	.15
--	5:06.9-68:28	--	1838?	14.3x 9.4	0	2095	0	1472	0	0	| Ed		18		25NE	.16
D110	5:14.3-69:31	39	--	4.8x 8.4	8.0	233	4	121	9	5	L40	25x38	23		14E	.15
D91	5:10.2-71:29	--	--	5.1x 4.2	3.0	103	3	66	7	4	L42Ed	30x34	15	5:13.5-71:10	30SW	.12
--	5:10.6-70:14	--	--	5.8x 5.4	0	317	0	49	0	0	L41Ed	36x30	18	5:12.6-70:32	23NW	.15
D90	5:10.7-67:10	32	--	6.0x 9.5	4.0	208	3	80	7	3	L5	53x40	25	5:11.8-67:05	9SW	.11
D95,96	5:11.4-69:10	33	--	4.8x 8.4	0.5	96	1	50	2	1	L39	38x32	30	5:11.3-69:05	5S	.16
D110	5:14.3-69:31	39	--	4.8x 8.4	8.0	233	4	121	9	5	L43Ed	34x26	23	5:18.6-69:29	31W	.15
D132B	5:18.5-69:13	41	1910	6.0x 9.5	40.0	3760	1	1154	7	3	|		15		16N	.15*
N122	5:20.3-69:34	46	--	2.4x 2.4	0.1	5	3	6	2	2	|		19		13SE	.12
N32	5:15.9-68:02	--	--	2.4x 2.4	0.3	9	5	--	--	5	L7	38x27	20	5:16.5-68:11	10NW	.20
--	5:16.8-67:31	--	--	4.0x 2.8	0	89	0	27	0	0	L6 Ed	29x36	18	5:13.5-67:36	24E	.14
--	5:17.7-70:21	--	--	2.7x 2.4	0	52	0	13	0	0	L28	30x36	15	5:19.4-70:10	16SW	.11
--	5:19.1-68:16	--	--	3.6x 3.3	0	175	0	40	0	0	L9 Ed	38x43	25	5:21.7-68:01	24SE	.19
--	5:20.4-67:21	--	--	6.3x 6.6	0	290	0	129	0	0	L11Ed	30x38	18	5:22.9-67:14	19W	.13
--	5:22.9-67:12	--	--	7.5x 5.1	0	95?	0	169?	0	0	|		20		2S	.11

Table 3. High UF, Low HInd (Cont. p. 2)

DEM or N No.	RA(1950)DEC	LH No.	NGC No.	ΔδxΔα Size	HA	L-Filter UF	L-Filter HInd.	C-Filter UF	C-Filter HInd.	100x Mean HInd.	Cloud No.	ΔδxΔα Size	Fl.	RA(1950)DEC	Dist. to UF	RE
D142	5:21.6-65:48	45	--	11.9x10.7	10.0	2261	1	920	2	1	L10	24x24	13	5:22.6-65:38	12SW	.18
N126	5:21.9-69:05	44	--	2.4x 3.6	0.3	13	1	7	6	2	L29	43x36	20	5:23.5-69:01	12W	.15
--	5:31.1-68:45	64?68?	--	7.8x 7.8	0	4623	0	--	0	0	L31	40x32	20	5:32.4-68:27	18S	.20
-	5:31.7-68:50	68	--	6.0x 3.6	0	132	0	4	0	0	⌊ Ed		23		23S	.20
[illegible]	5:32.0-67:33	--	2011	8.4x 9.2	0.8	2887?	0	438	0	0	L13	34x30	17	5:32.1-67:50	17N	.10
-	5.36.2-68:55	85,89	2042	9.3x 9.3	0	19866	0	7800	0	0	L32	36x53	28	5:40.0-68:53	27W	.42
[illegible]	5:36.5-68:57	85?89	2042	10.7x 6.0	0	8352	0	4331	0	0	|		29		25W	.42
--	5:42.4-69:13	111	2100	7.2x 8.4	0	4214	0	1320	0	0	⌊ Ed		37		27SE	.31
--	5:37.6-67:44	--	--	4.5x 5.1	0	61	0	99	0	0	L14	28x35	30	5:35.9-67:38	14E	.12
N216	5:41.6-70:55	--	--	3.6x 3.6	0.6	55	3	--	--	3	L50	72x57	35	5:40.4-71:04	12NE	.28
--	5:44.6-66:38	--	--	3.0x 4.2	0	116	0	3	0	0	L16	44x43	15?	5:45.6-66:19	19S	.12

Table 4. IUE Measurements of LMC Stars

Object LH/NGC	100x HIND	HI	SWP Image	Exp.	Continuum Flux[1] 1300	1400	1500	Equivalent Width (Angstroms) Lyα	SiIII	CII	SiIV	CIV	1720	RE[2]	LWR Image	Exp.	Continuum Flux[1] 2325	2675	2900	EW MgII	Spec. Type[3]	N[HI] (x10^{20}/cm^2)
High Hydrogen Index:																						
N51BE	114	23	4129	30m	1.44*	1.19*	1.36*	8.5	3.4	2.0	0.3	15.1e	2.4	.11	3658	15m	.340	.210	.149	5.2	O4-7 V	(H) 9.9
LH55																						
N55,A	65	10	4038	60	2.94	1.85	2.13	11.7	3.8	2.6	0.8?	0.0	2.4	.05	3580	55	.340	.246	.256	1.4	B8-9	(P) —
LH72																						
N56,59	134	30	4057	80	2.12	1.96	1.96	17.e	3.3	3.4	1.3?	0.0	2.3	.11	3595	40	.641	.549	.503	5.3	B7e	(P) —
LH88																						
N70	69	20	4126	40	1.57*	1.40*	1.44*	12?	2.0	1.4	4.8?	5.0?	4.1	.12	3616	30	.548	.358	.338	2.6	O4-B1 I	(H) 19.8
LH114																						
N70	69	20	4128	15	2.13	1.96	1.96	4.5	2.7	1.9	6.6	5.5e	3.4	.12	3657	10	.500	.374	.314	5.3	O4-B1 I	(H) 2.8
LH114																						
Low Hydrogen Index:																						
N1818	0	15	4123	100	2.18	1.91	1.75	12.	4.8	2.2	2.2	0.8	3.4	.17	3615	30	.786	.750	.625	5.6	B2:III-V	(H) 19.8
LH64	0	18	4061	40	1.23*	1.20*	1.29*	9.5?	1.9	1.0	2.2?	3.8?	1.7	.09	3600	20	.565	.418	.356	4.4	B1 III-V	(H) 12.4
LH64	0	18	4062	10	3.30	2.38	2.16	13.7	3.8	1.8	4.3	2.0	0.8	.09	3601	10	.666	.500	.406	6.2	B1 III-V	(H) 25.7
D232	9	19	4059	30	1.72†	2.06†	1.75†	32?	2.6	1.5	1.7?	1.0?	1.8	.14	3598	15	.565	.243	.133		B5?	(P) —
LH74#1																						
D232	9	19	4059	30	0.86†	1.80†	1.75†	71?	5.0	10.0	1.0?	7.0?	4.	.14	3598	15	.354	.411	.452		B9?	(P) —
LH74#2																						
LH77	0	15	4124	60	2.16	1.86	1.71	16.	4.7	1.9	3.4	1.5	1.9	.11	3655	30	.746	.706	.680	5.5	B1 III-V	(H) 35.
N58	5	20	4130	40	3.01	2.39	2.19	6.	5.8	1.6	2.0	1.0?	4.2	.11	3659	20	.770	.552	.440	5.5	B1-3	(H) 4.9
LH79																						
LH89	0	29	4058	60	1.62†	1.16†	1.59†	22.e	4.0	3.3	11.2?	<1.5	4.9	.42	3596	30	.715	.755	.808	8.6	B1-2eIII-V	(H) —
LH111	0	39	4084	127	1.55	1.39	1.41	36.	4.1	2.8	2.2	1.3	2.5	.31	3597	50	.785	.826	.790	5.9	B1 III-V	(H) 178.
Medium Hydrogen Index:																						
D43	21	15	4127	30	1.87	1.52	1.82	0.	5.3	2.8	>1.0	<1.3	1.7	.09	3617	20	.490	.495	.466	5.3	B2-3	(H) —
LH15																						

Footnotes:

[1] In units of 10^{-14} erg/cm^2 Å relative to 1925Å.

[2] Color excess, E(B-V), from Lucke (1974) as interpolated by Page and Carruthers (1978).

[3] Spectral type inferred from far-UV line ratios by Henize (H) or Page (P).

Table 5. Continuum Flux Relative to 1925Å, Reddened KPA Models

Te	RE	1300Å	1400Å	1500Å	1925Å	2325Å	2675Å	2900Å
14000K	.00	1.805	1.705	1.543	1.000	0.667	0.531	0.460
14000K	.05	1.57	1.59	1.51	1.000	0.701	0.600	0.535
14000K	.10	1.37	1.49	1.48	1.000	0.738	0.678	0.624
14000K	.15	1.195	1.39	1.445	1.000	0.776	0.765	0.727
14000K	.36	0.670	1.053	1.33	1.000	0.963	1.275	1.385
16000K	.00	2.06	1.86	1.65	1.000	0.649	0.489	0.412
16000K	.05	1.79	1.73	1.615	1.000	0.682	0.552	0.478
16000K	.10	1.565	1.625	1.58	1.000	0.717	0.623	0.559
16000K	.15	1.363	1.52	1.545	1.000	0.755	0.705	0.650
16000K	.36	0.765	1.15	1.42	1.000	0.935	1.173	1.24
18000K	.00	2.30	2.00	1.757	1.000	0.630	0.454	0.374
18000K	.05	2.00	1.87	1.72	1.000	0.662	0.512	0.435
18000K	.10	1.745	1.75	1.68	1.000	0.696	0.578	0.507
18000K	.15	1.52	1.633	1.655	1.000	0.733	0.655	0.591
18000K	.36	0.853	1.235	1.51	1.000	0.909	1.09	1.125
20000K	.00	2.455	2.125	1.853	1.000	0.612	0.427	0.346
20000K	.05	2.14	1.98	1.81	1.000	0.643	0.482	0.402
20000K	.10	1.86	1.86	1.78	1.000	0.676	0.545	0.470
20000K	.15	1.625	1.735	1.735	1.000	0.713	0.615	0.547
20000K	.36	0.910	1.315	1.595	1.000	0.893	1.025	1.04
25000K	.00	2.96	2.34	2.025	1.000	0.575	0.376	0.294
25000K	.05	2.58	2.18	1.98	1.000	0.604	0.424	0.342
25000K	.10	2.245	2.04	1.94	1.000	0.635	0.479	0.399
25000K	.15	1.96	1.91	1.90	1.000	0.670	0.542	0.465
25000K	.36	1.10	1.445	1.745	1.000	0.830	0.903	0.885

Table 5. (Cont.)

Te	RE	1300Å	1400Å	1500Å	1925Å	2325Å	2675Å	2900Å
30000K	.00	3.135	2.44	2.077	1.000	0.555	0.350	0.267
30000K	.05	2.72	2.28	2.03	1.000	0.583	0.395	0.310
30000K	.10	2.38	2.13	1.99	1.000	0.614	0.446	0.363
30000K	.15	2.07	1.99	1.94	1.000	0.645	0.504	0.422
30000K	.36	1.16	1.51	1.79	1.000	0.800	0.840	0.805
35000K	.00	3.08	2.48	2.037	1.000	0.565	0.355	0.271
35000K	.05	2.68	2.31	1.99	1.000	0.593	0.400	0.314
35000K	.10	2.34	2.17	1.95	1.000	0.625	0.452	0.368
35000K	.15	2.04	2.025	1.905	1.000	0.657	0.511	0.428
35000K	.36	1.14	1.535	1.75	1.000	0.815	0.851	0.815
40000K	.00	3.32	2.66	2.135	1.000	0.558	0.346	0.262
40000K	.05	2.88	2.48	2.085	1.000	0.585	0.390	0.304
40000K	.10	2.52	2.32	2.045	1.000	0.617	0.441	0.356
40000K	.15	2.20	2.17	2.00	1.000	0.649	0.498	0.414
40000K	.36	1.23	1.645	1.84	1.000	0.805	0.830	0.790
45000K	.00	3.42	2.735	2.175	1.000	0.550	0.339	0.255
45000K	.05	2.97	2.55	2.125	1.000	0.578	0.382	0.296
45000K	.10	2.59	2.38	2.08	1.000	0.608	0.432	0.346
45000K	.15	2.26	2.23	2.035	1.000	0.640	0.488	0.403
45000K	.36	1.27	1.69	1.87	1.000	0.794	0.812	0.768
50000K	.00	3.48	2.80	2.21	1.000	0.542	0.332	0.249
50000K	.05	3.025	2.61	2.16	1.000	0.569	0.374	0.289
50000K	.10	2.64	2.445	2.16	1.000	0.600	0.423	0.338
50000K	.15	2.30	2.29	2.07	1.000	0.630	0.478	0.394
50000K	.36	1.29	1.73	1.92	1.000	0.782	0.795	0.750

Table 6. Match of Spectral Type, KPA Continuum Flux, and Color Excess

LH No.	Measured RE	Measured Type	Expected Te	Continuum Match 1300-1925Å Te	1300-1925Å RE	1925-2900Å Te	1925-2900Å RE	
72	.05*	B8-9?	13000K	30000 40000	.05 .10	>50000	.00?	
64	.09*	B1	24000	50000	.05	50000	.10	
79	.11*	B1-3	22000	50000	.05	20000	.10	
114	.12	O4-B1	32000	35000 40000	.05 .10	50000 40000	.05 .05	
88	.11	B7e	14500	30000	.15	30000	.15	
N1818	.17	B2	22000	20000	.05	20000 14000	.20 .10	
77	.11	B1	24000	20000	.05	14000	.10	
89	.42*	B1-2e	23000	16000 18000	.15 .36	18000	.20	Underexp.
15	.09*	B2-3	20000	18000	.15	20000	.05?	
111	.31*	B1	24000	14000 20000	.10? .36?	14000 20000	.17? .20	
55	.11	O4-07	38000	16000	.36? .20?	>50000	.00?	
74#1	.14*	B5?	16000	20000	.10?	>50000	.00?	Underexp.
74#2	.14*	B9?	12000	20000	.10?	>50000	.05?	Underexp.

REFERENCES

Ardeberg, A., Brunet, J. P., Maurice, E., and Prevot, L. 1972, Astron. & Astrophys. Suppl., 6, 249.

Bless, R. C. and Savage, B. D., 1972, Ap. J., 171, 293.

Bohlin, R. C., 1975, Ap. J., 200, 402.

Bohlin, R. C., Savage, B. D., and Drake, J. F., 1978, Ap. J., 224, 132.

Bohlin, R. C., Holm, A. V., Savage, B. D., Snijders, M. A. J., and Sparks, W. M., 1980, Astron. & Astrophys., 85, 1.

Borgman, J. and Danks, A. C., 1977, Astron. & Astrophys., 54, 41.

Carruthers, G. R., 1970, Space Sci. Revs., 10, 459.

Carruthers, G. R., Heckathorn, H. M., and Opal, C. B., 1978, Ap. J., 225, 346.

Carruthers, G. R. and Page, T., 1972, Chap. 13 in Apollo 16 Prelim. Sci. Report, NASA SP-315.

Carruthers, G. R. and Page, T., 1977, Ap. J., 211, 723.

Carruthers, G. R., 1973, Appl. Optics, 12, 2501.

Code, A. D. and Meade, M. R., 1979, Ap. J. Supp., 39, 195.

Code, A. D., Holm, A. V., and Bottemiller, R. L., 1980, Ap. J. Supp., 43, 501.

Davies, R. D., Elliott, K. H., and Meaburn, J., 1976, Mem. R. Astr. Soc., 81, 89.

de Boer, K. S., Koornneef, J., and Savage, B. D., 1980, Ap. J., 236, 769.

Doherty, L., Henize, K. G., and Aller, L. H., 1956, Ap. J. Supp., 2, 345.

Henize, K. G., 1956, Ap. J. Supp., 2, 315.

Henry, R. C., 1977, Ap. J. Supp., 33, 451.

Jenkins, E. B., 1970, in Ultraviolet Stellar Spectra and Ground-Based Observations, (Houziaux, L. and Butler, H. E., Eds., Reidel, D., Dortrecht), p. 281.

Jenkins, E. B. and Savage, B. D., 1974, Ap. J., 187, 243.

Koornneef, J., 1978, Astron. & Astrophys., 64, 179.

Koornneef, J. and Mathis, J. S., 1980, preprint.

Kurucz, R. L., Peytremann, E., and Avrett, E. H., 1974, Blanketed Model Atmospheres for Early-Type Stars, Smithsonian Institute, Washington, D. C.

Lucke, P. B. and Hodge, P. W., 1970, Astron. Jour., 75, 171.

Lucke, P. B., 1974, Ap. J. Supp., 28, 73.

McGee, R. X. and Milton, J. A., 1966, Australian Jour. Phys., 19, 343.

McGee, R. X., Brooks, J. W., and Batchelor, R. A., 1972, Australian Jour. Phys., 25, 581.

Nandy, K., Morgan, D. H., Willis, A. J., Wilson, R., Gondhalekhar, P. M., and Houziaux, L., 1980, Nature, 283, 725.

Page, T. and Carruthers, G. R., 1977, COSPAR Space Research, Vol. XVII (Pergamon, New York), p. 74.

Page, T., Carruthers, G. R., and Hill, R. E., 1978, S201 Catalog of Far-UV Objects, NRL Report 8173.

Page, T. and Carruthers, G. R., 1978, S201 Far-UV Atlas of the LMC, NRL Report 8206.

Pottasch, S. R., 1965, Vistas in Astronomy, Vol. 6 (Beer, A., Ed., Pergamon, New York) p. 149.

Savage, B. D., 1975, Ap. J., 199, 92.

Savage, B. D. and Jenkins, E. B., 1972, Ap. J., 172, 491.

Spitzer, L., Jr., 1978, Physical Processes in the Interstellar Medium (Wiley/Interscience, New York).

Walborn, N. R., 1977, Ap. J., 215, 53.

Witt, A. N. and Johnson, M. W., 1973, Ap. J., 181, 363.

York, D. G., 1976, Mem. Soc. Astr. Italiana, 47, 493.

THORNTON PAGE, Code SN, NASA Johnson Space Center, Houston, Texas 77058

GEORGE R. CARRUTHERS, Code 4143, Naval Research Laboratory, Washington, D.C. 20375

FIGURE CAPTIONS

1. Far-ultraviolet (1230-1600 Å) images of the Large Magellanic Cloud obtained with the S201 Far Ultraviolet Camera: (Top) 3 min exposure, (Bottom) 30 min exposure. The shorter exposure shows the prominent OB associations and individual UV-bright stars. The longer exposure reveals the general distribution of less luminous OB stars. Note the apparent sharp outer boundary of the UV star distribution (arrows). North is up.

2. Isodensity contour plot generated for the 10 min 1250-1600 Å exposure on the LMC. Contour interval is 0.10 D. The vertical and horizontal axes are x and y scan coordinates, in rasters. Superimposed on the plot is an approximate RA-DEC (1950) grid, with north to the right. Positions of LH associations, Henize nebulae (N numbers), and foreground SAO stars are indicated.

3. Contours of the Hydrogen Index (times 100) in the Large Magellanic Cloud. Contour lines are for 100 H Ind = 10, 20, 50, and 100. The vertical and horizontal axes are as for Fig. 2.

4. Contour plot of E(B-V) in the LMC, based on values given by Lucke (1974). These were used for correcting the far UV and Hα brightnesses for interstellar extinction using the curve of Nandy et al. (1980) in Fig. 5. Axes, orientation, and scale are as for Fig. 3.

5. Interstellar extinction curves typical of the local regions of our galaxy (Bless and Savage 1972) and for the 30 Doradus region of the LMC (Nandy et al. 1980). C and L indicate the effective wavelengths of the S201 imagery with CaF_2 corrector (1400 Å) and with LiF corrector (1300 Å).

6. Plot of our estimates of Hα brightness × (arc min)^2 for emission nebulae observed by Davies et al. (1976) vs. Hα brightnesses of Henize (1956) for objects in common.

7. Photon flux vs. wavelength, normalized to 5500 Å, for unreddened stars of various effective temperatures based on the model atmosphere calculations of Kurucz, Peytremann, and Avrett (1974).

8. Integrated flux ratios vs. effective temperature, based on the model atmosphere flux distributions of Kurucz et al. (1974). The ratios plotted are: ILi/Vis = (1050-1600 Å)/(5000-6000 Å), ILi/ICa = (1050-1600 Å)/(1250-1600 Å), LyC/Vis = (λ < 912 Å)/(5000-6000 Å), and LyC/ILi = (λ < 912 Å)/(1050-1600 Å).

9. Contours of neutral hydrogen 21-cm emission in the LMC, based on the measurements of McGee and Milton (1966). Contour lines are for 20, 30, 40, and 50 flux units, where 1 flux unit = 1.76 K brightness temperature at 21 cm. Errors are about ± 10%, and the angular resolution is about 14.5 arc min. Coordinates, orientation, and scale are as for Figs. 3 and 6.

10. IUE spectra, corrected for nonlinearity and distortion but not for instrumental spectral response, in the association LH 114. The large aperture was used to obtain a spectrum of a star in the association (Top) and the foreground geocoronal Lα emission near the star was observed simultaneously using the small aperture (Bottom). The small aperture Lα intensity was scaled up to the value appropriate for the large aperture and subtracted from the large aperture spectrum.

11. Continuum fluxes vs. wavelength, relative to that at 1925 Å, for LMC stars observed with IUE. These, and other data on the observed stars, are listed in Table 4.

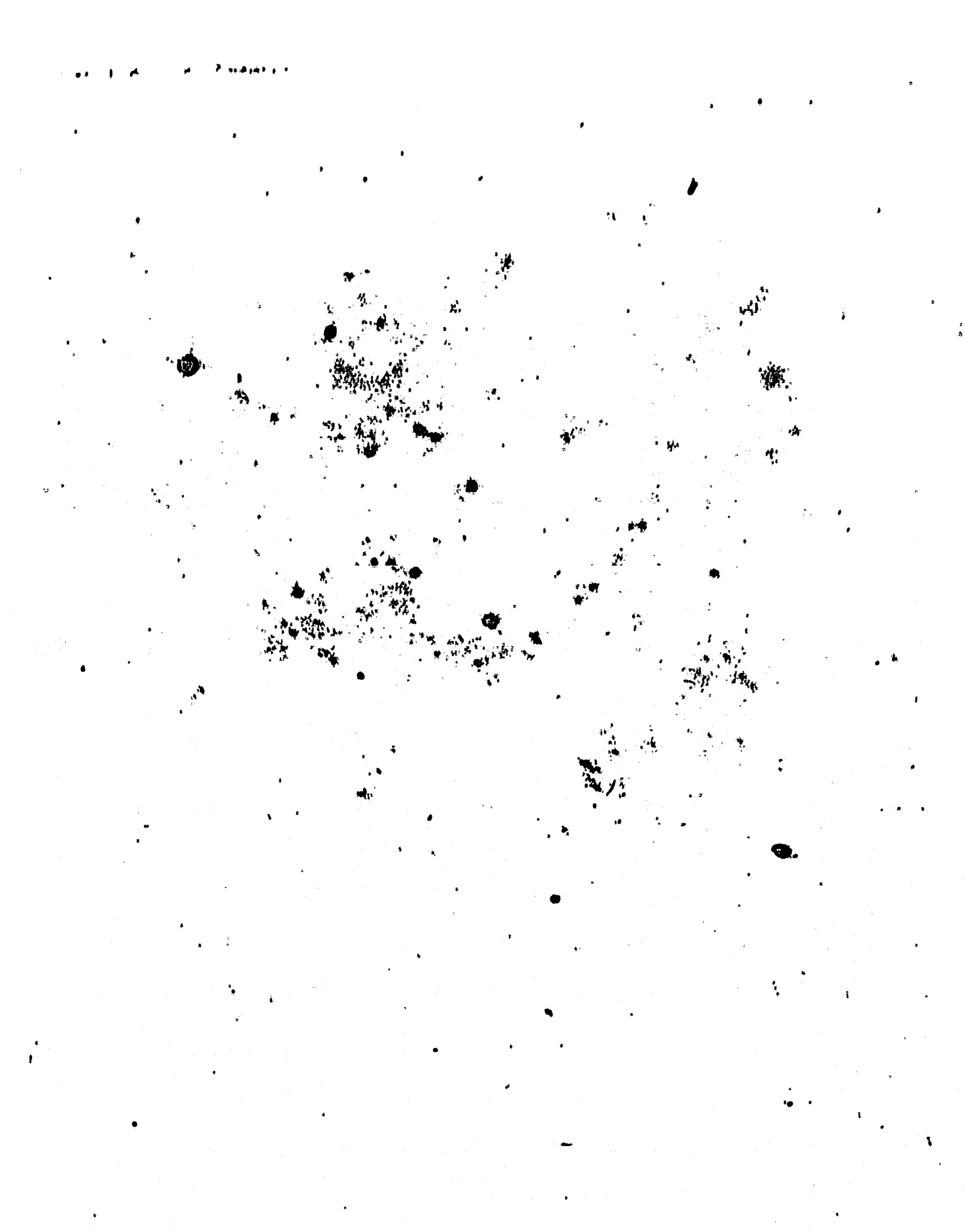

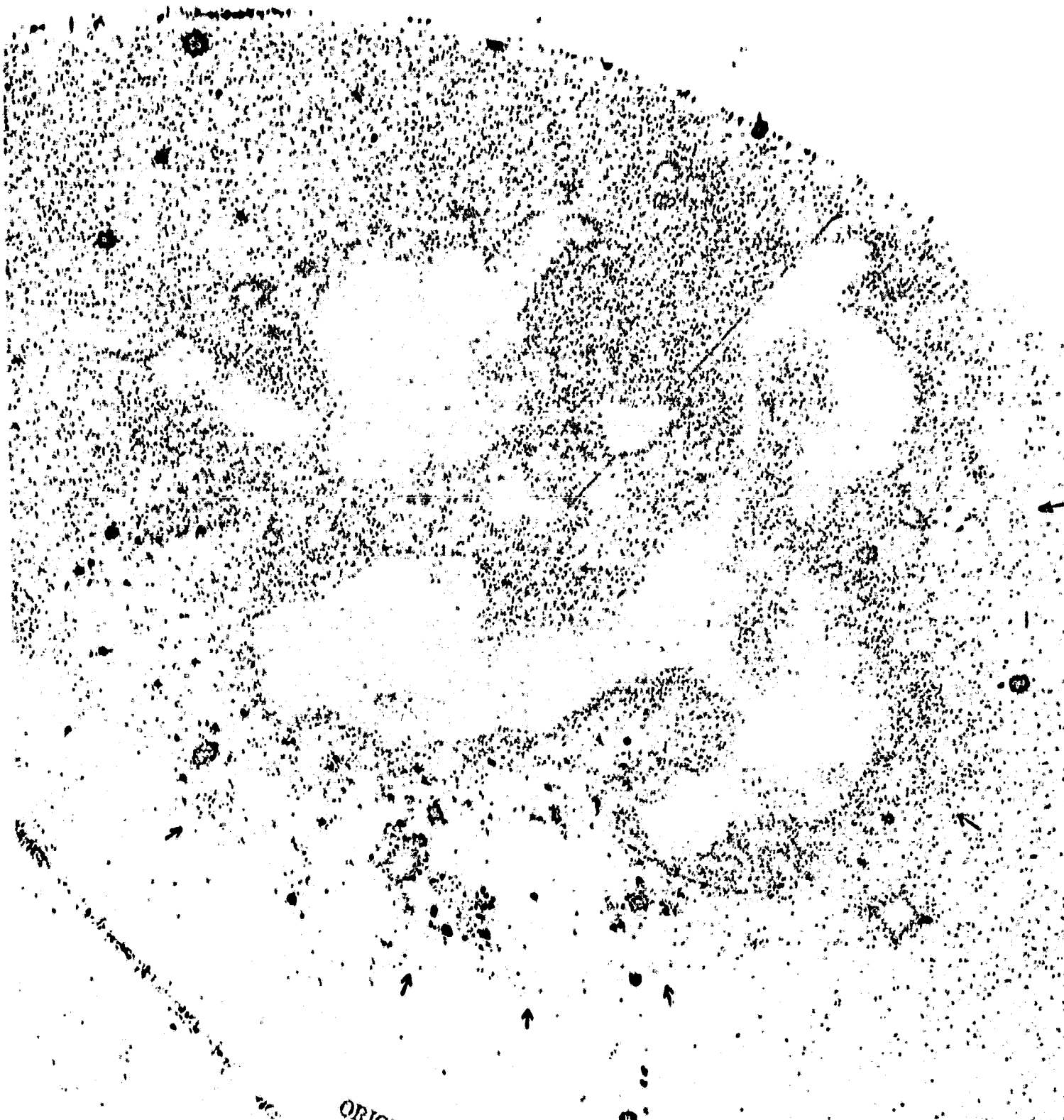

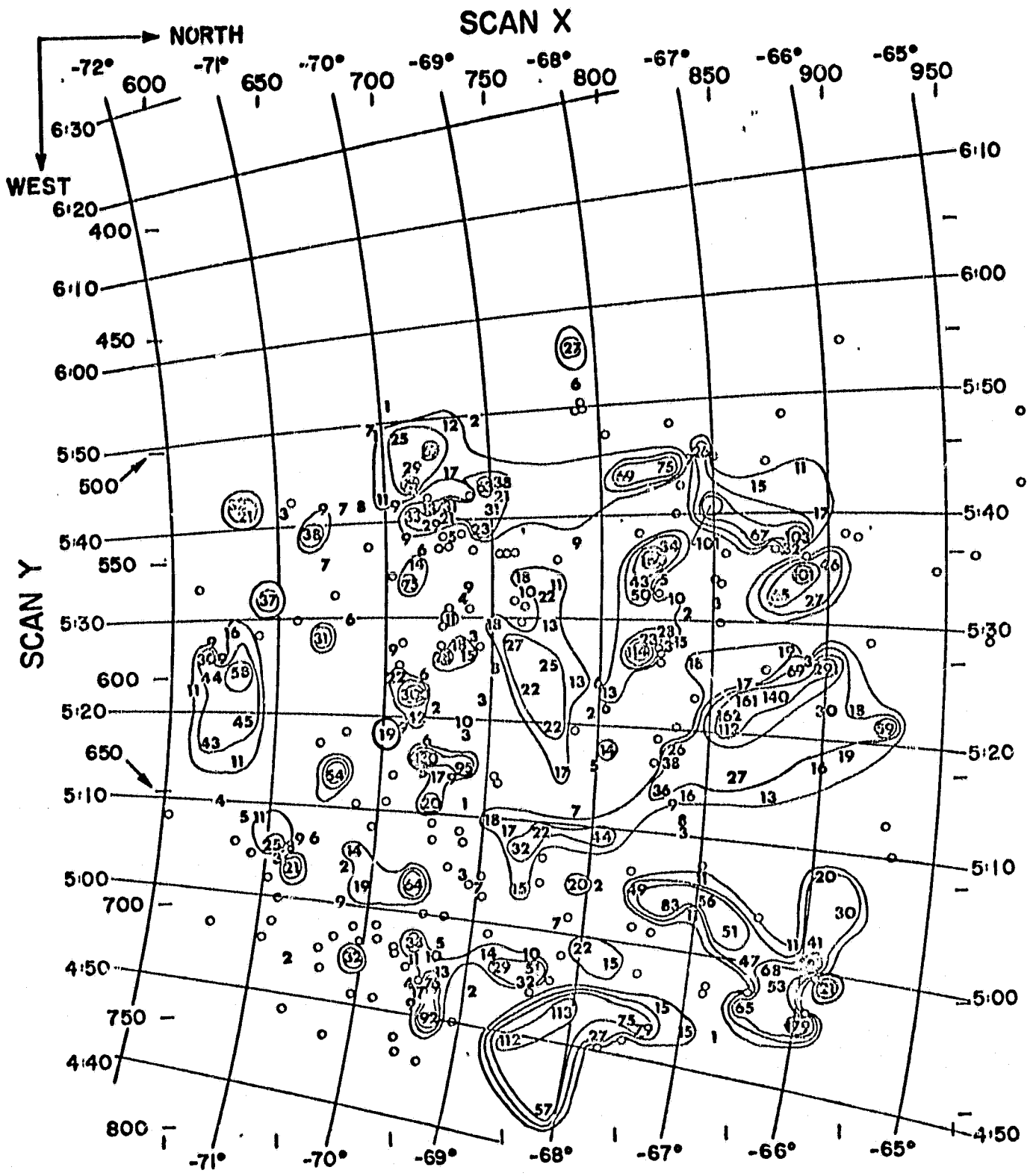

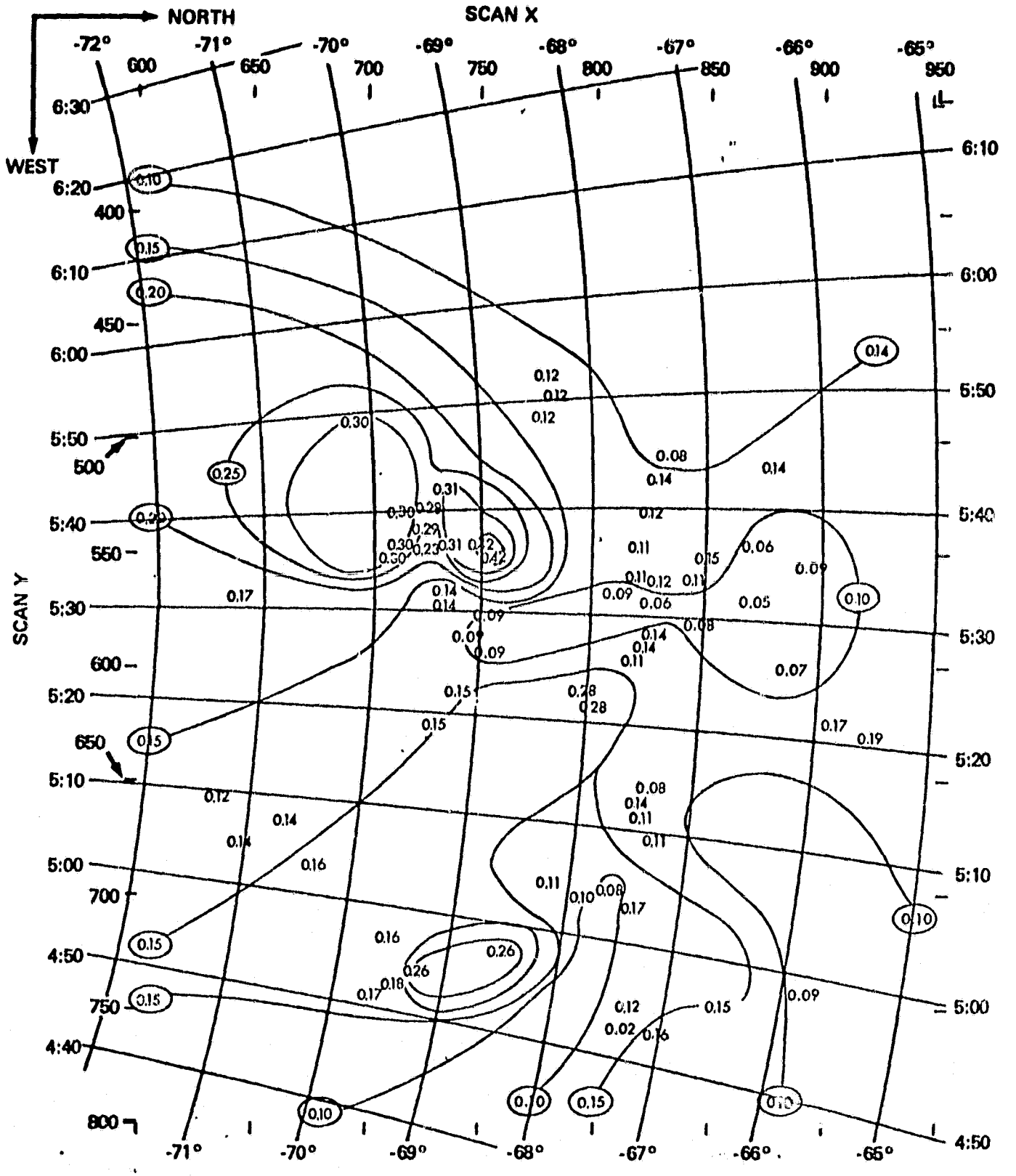
NORTH
SCAN X
WEST
SCAN Y
-72°
-71°
-70°
-69°
-68°
-67°
-66°
-65°
600
650
700
750
800
850
900
950
6:30
6:20
6:10
6:00
5:50
5:40
5:30
5:20
5:10
5:00
4:50
4:40
400
450
500
550
600
650
700
750
800
6:10
6:00
5:50
5:40
5:30
5:20
5:10
5:00
4:50
0.10
0.15
0.20
0.25
0.30
0.14
0.12
0.08
0.31
0.28
0.29
0.23
0.42
0.11
0.06
0.09
0.17
0.05
0.07
0.19
0.16
0.26
0.18
0.02

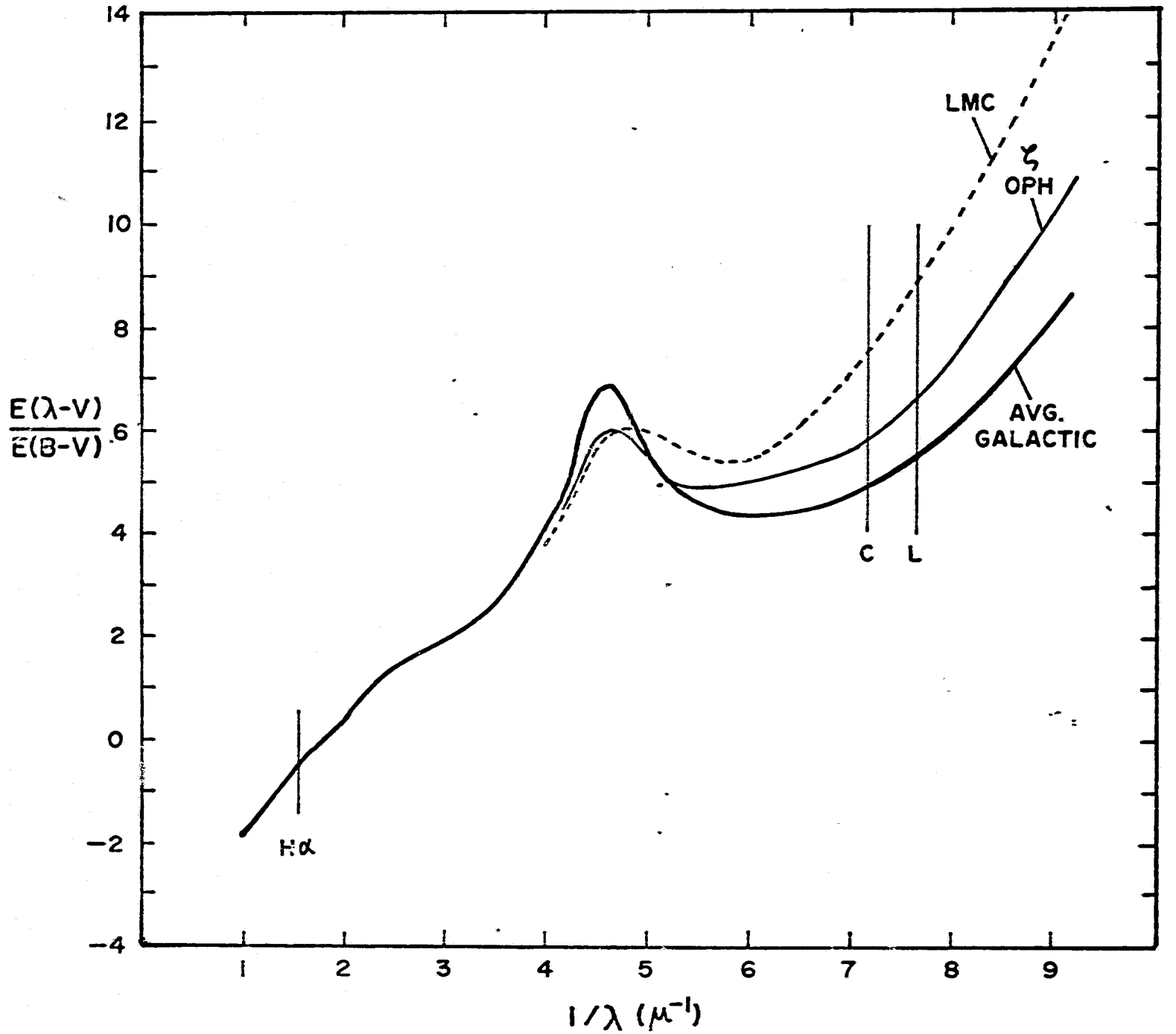
14
12
10
8
6
4
2
0
−2
−4
E(λ-V)
E(B-V)
1
2
3
4
5
6
7
8
9
1/λ (μ⁻¹)
LMC
ζ
OPH
AVG.
GALACTIC
C
L
Hα

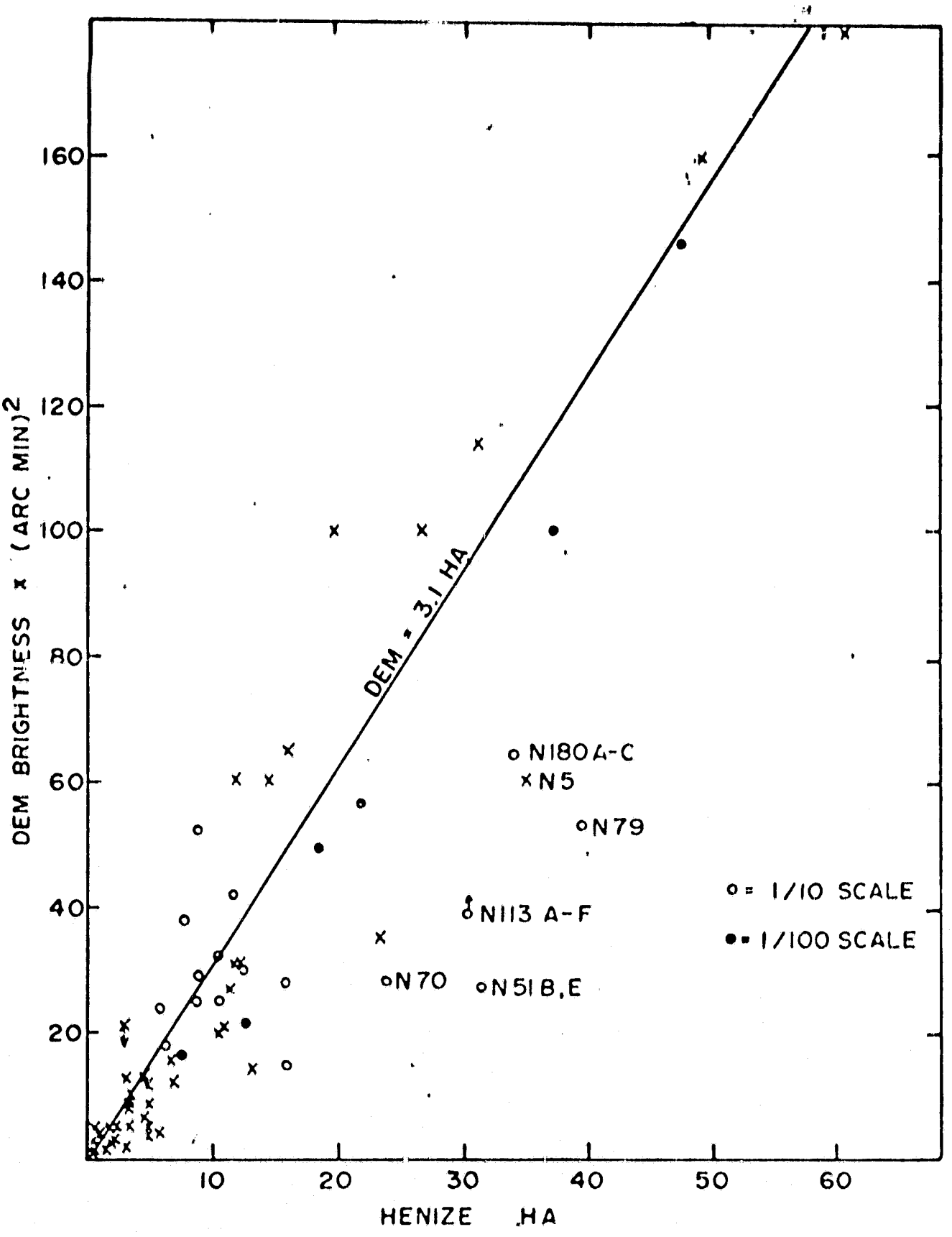
OEM BRIGHTNESS x (ARC MIN)^2
HENIZE HA
OEM = 3.1 HA
N180A-C
N5
N79
N113 A-F
N70
N51B,E
o = 1/10 SCALE
• = 1/100 SCALE
20
40
60
80
100
120
140
160
10
20
30
40
50
60

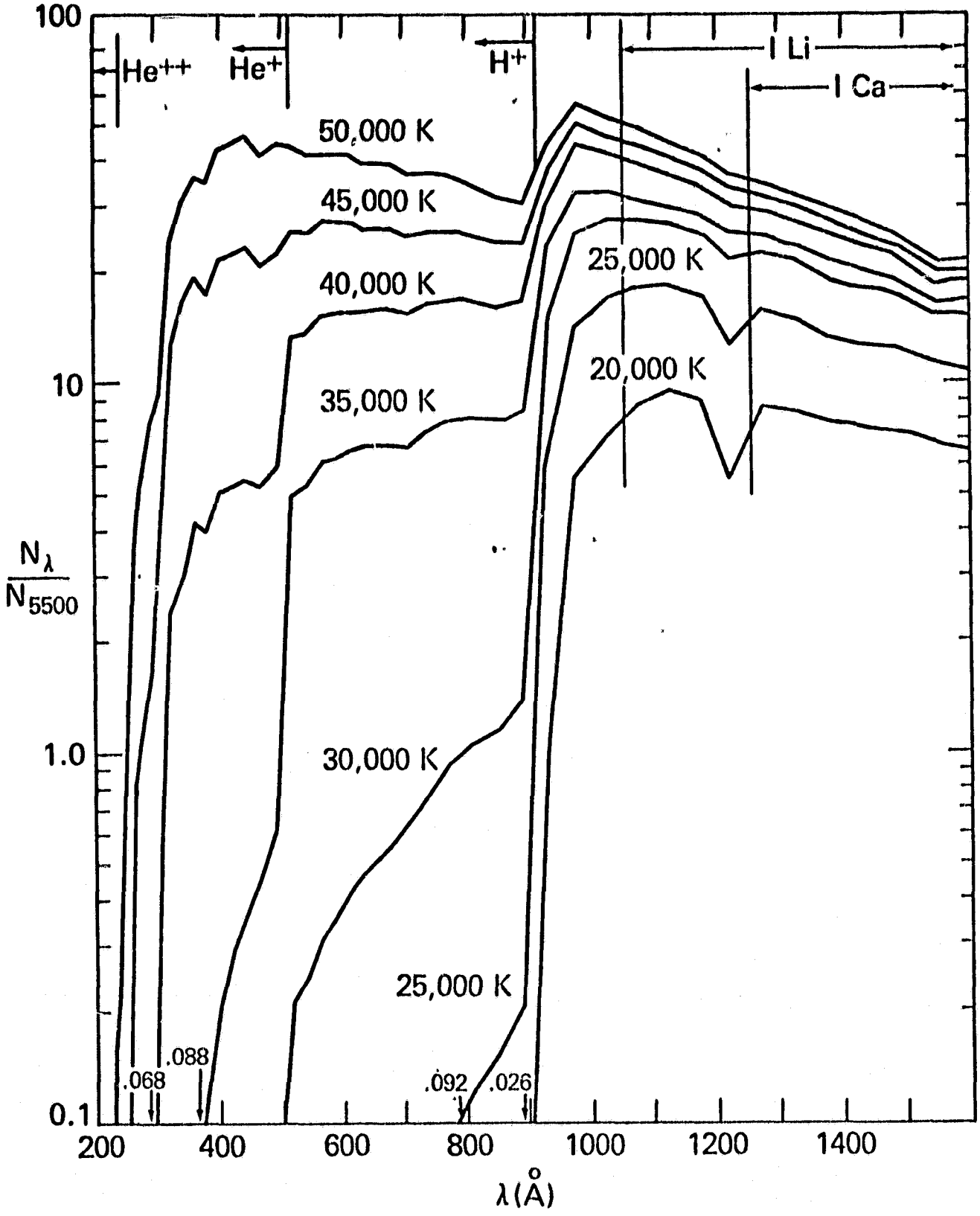
100
10
1.0
0.1
$\frac{N_\lambda}{N_{5500}}$
He++
He+
H+
I Li
I Ca
50,000 K
45,000 K
40,000 K
35,000 K
30,000 K
25,000 K
25,000 K
20,000 K
.068
.088
.092
.026
200
400
600
800
1000
1200
1400
λ(Å)

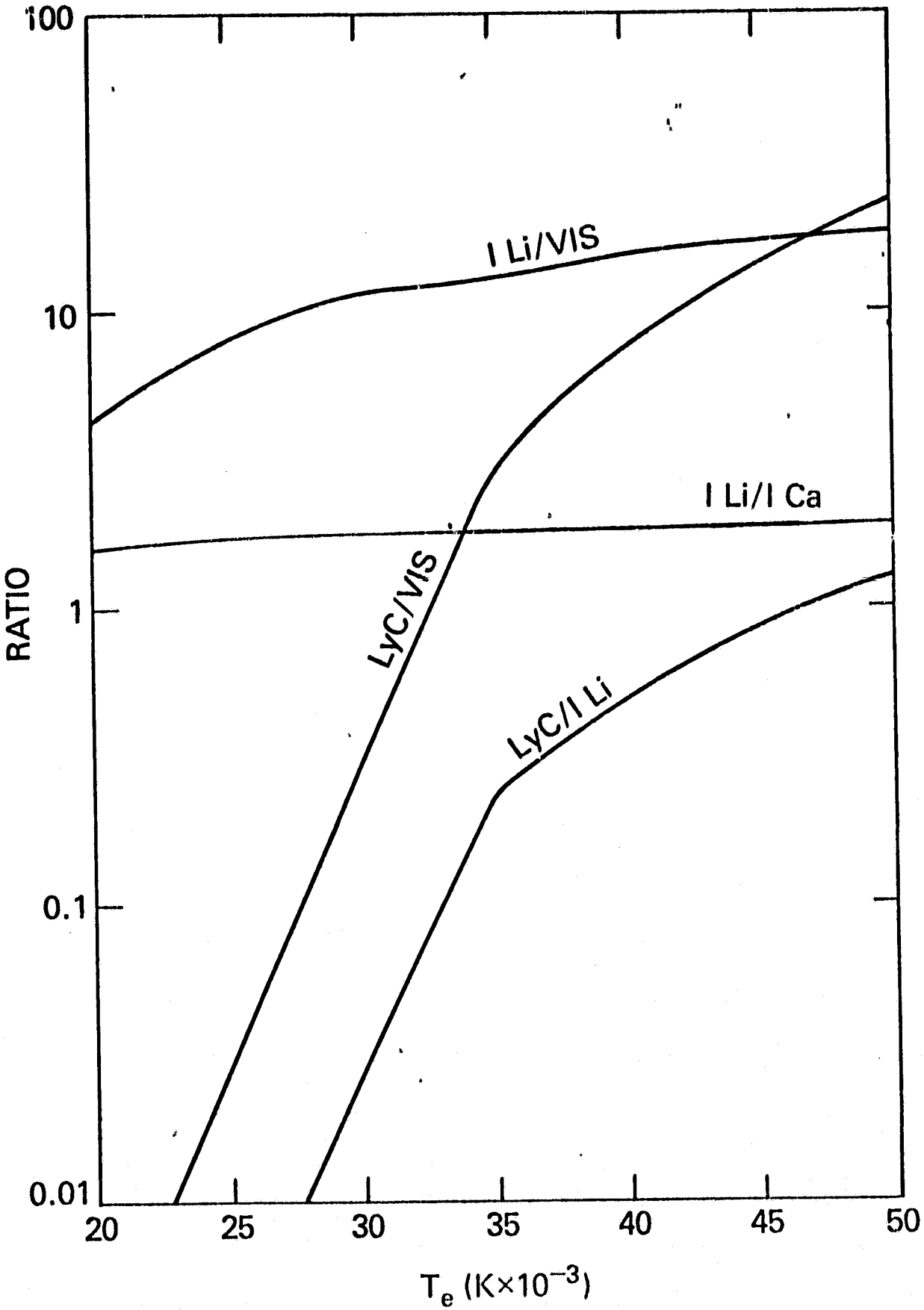
100
10
1
0.1
0.01
RATIO
I Li/VIS
I Li/I Ca
LyC/VIS
LyC/I Li
20
25
30
35
40
45
50
T_e (K×10^{-3})

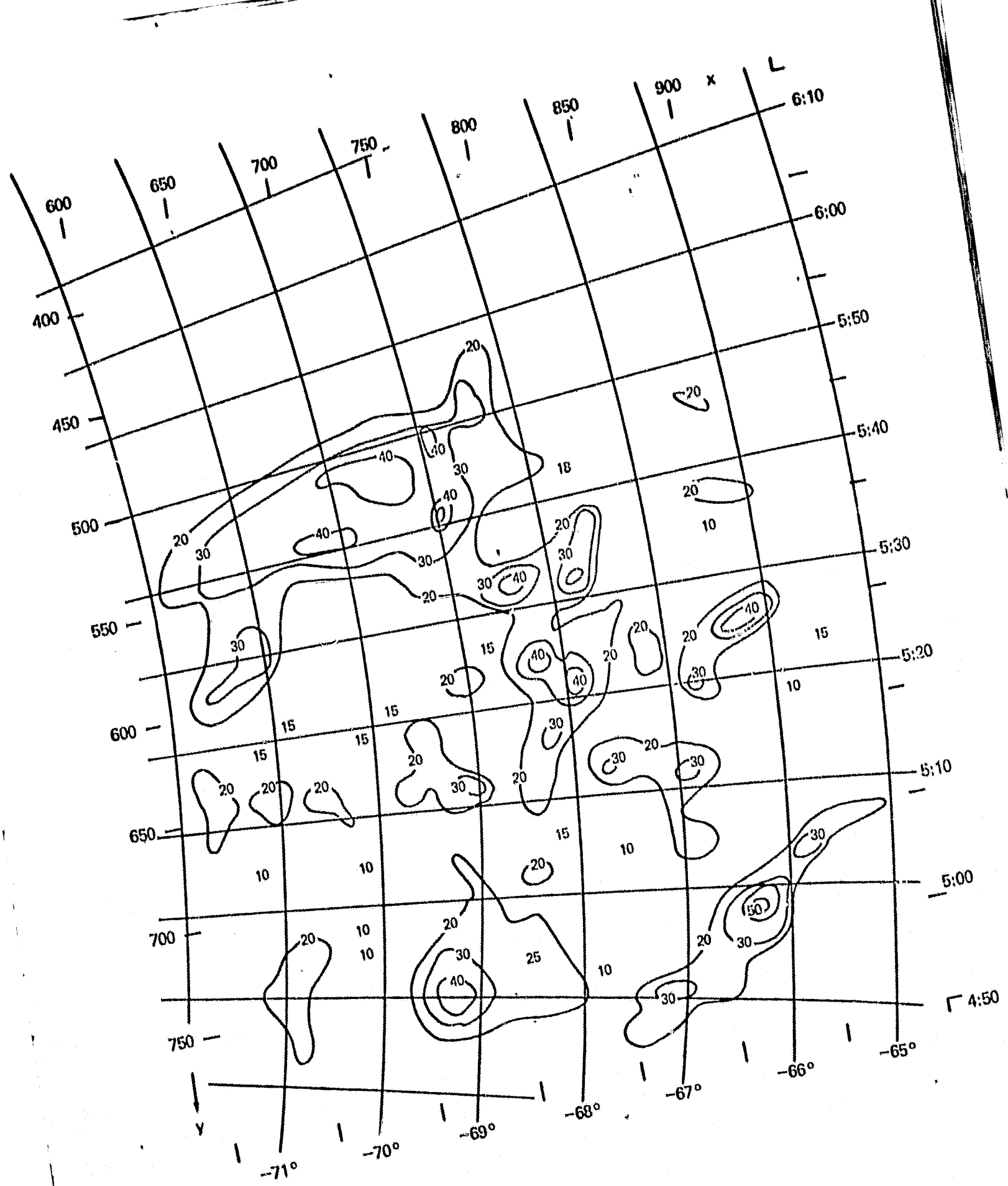

ORIGINAL PAGE IS
OF POOR QUALITY

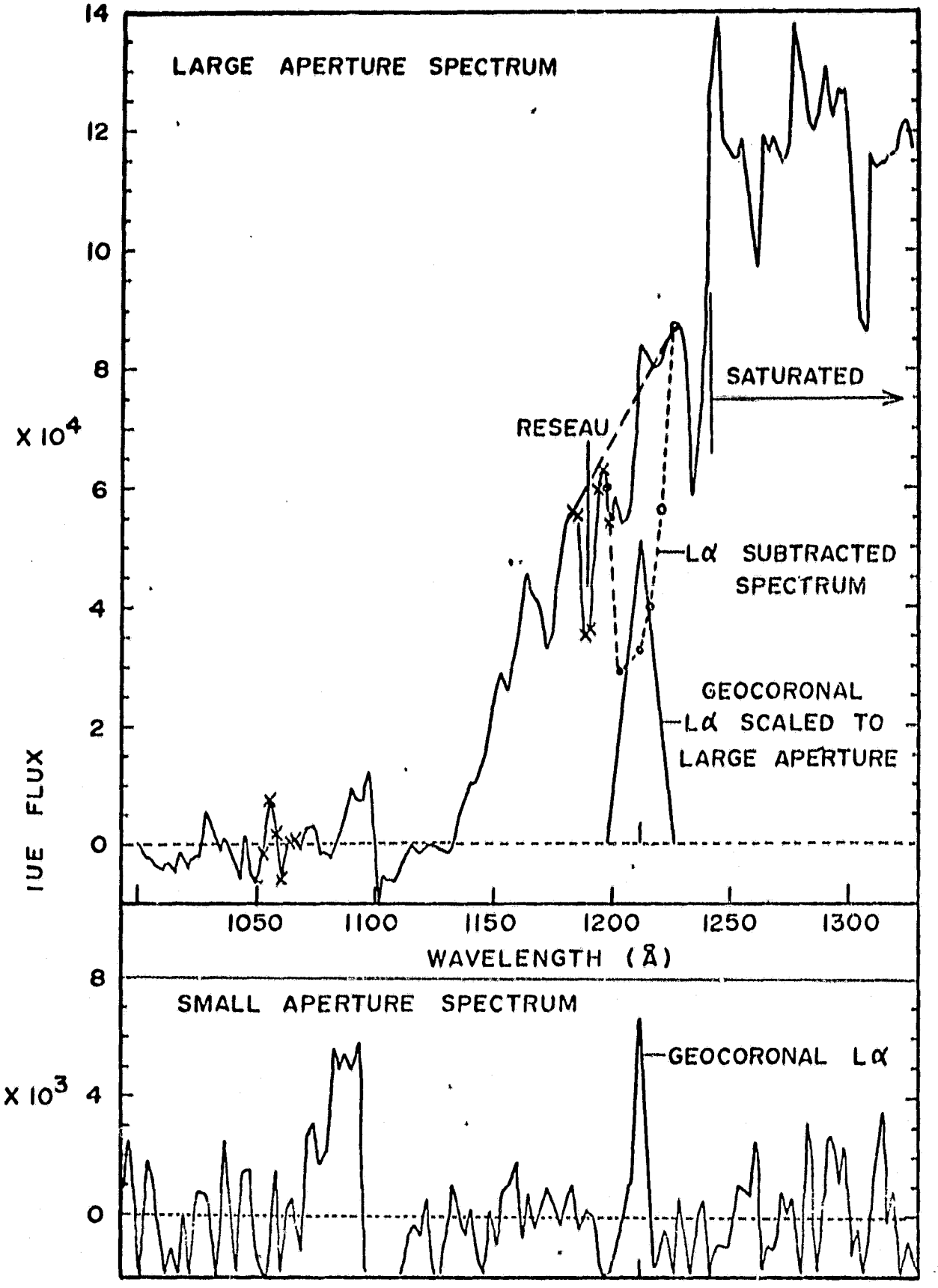
LARGE APERTURE SPECTRUM
SATURATED
RESEAU
Lα SUBTRACTED SPECTRUM
GEOCORONAL Lα SCALED TO LARGE APERTURE
X 10^4
IUE FLUX
14
12
10
8
6
4
2
0
1050
1100
1150
1200
1250
1300
WAVELENGTH (Å)
SMALL APERTURE SPECTRUM
GEOCORONAL Lα
X 10^3
8
4
0

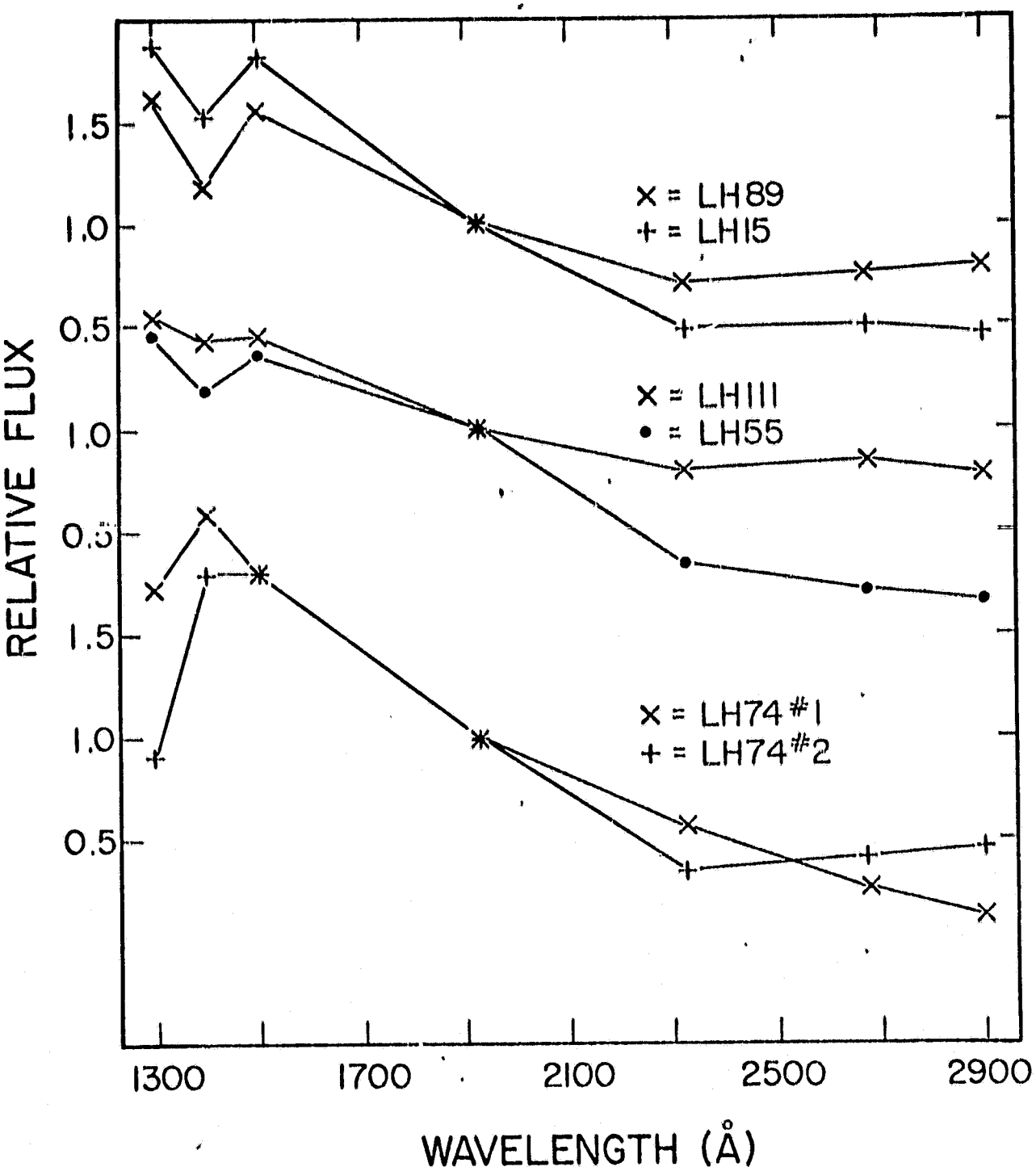
RELATIVE FLUX
1.5
1.0
0.5
1.0
0.5
1.5
1.0
0.5
× = LH89
+ = LH15
× = LH111
• = LH55
× = LH74 #1
+ = LH74 #2
1300
1700
2100
2500
2900
WAVELENGTH (Å)

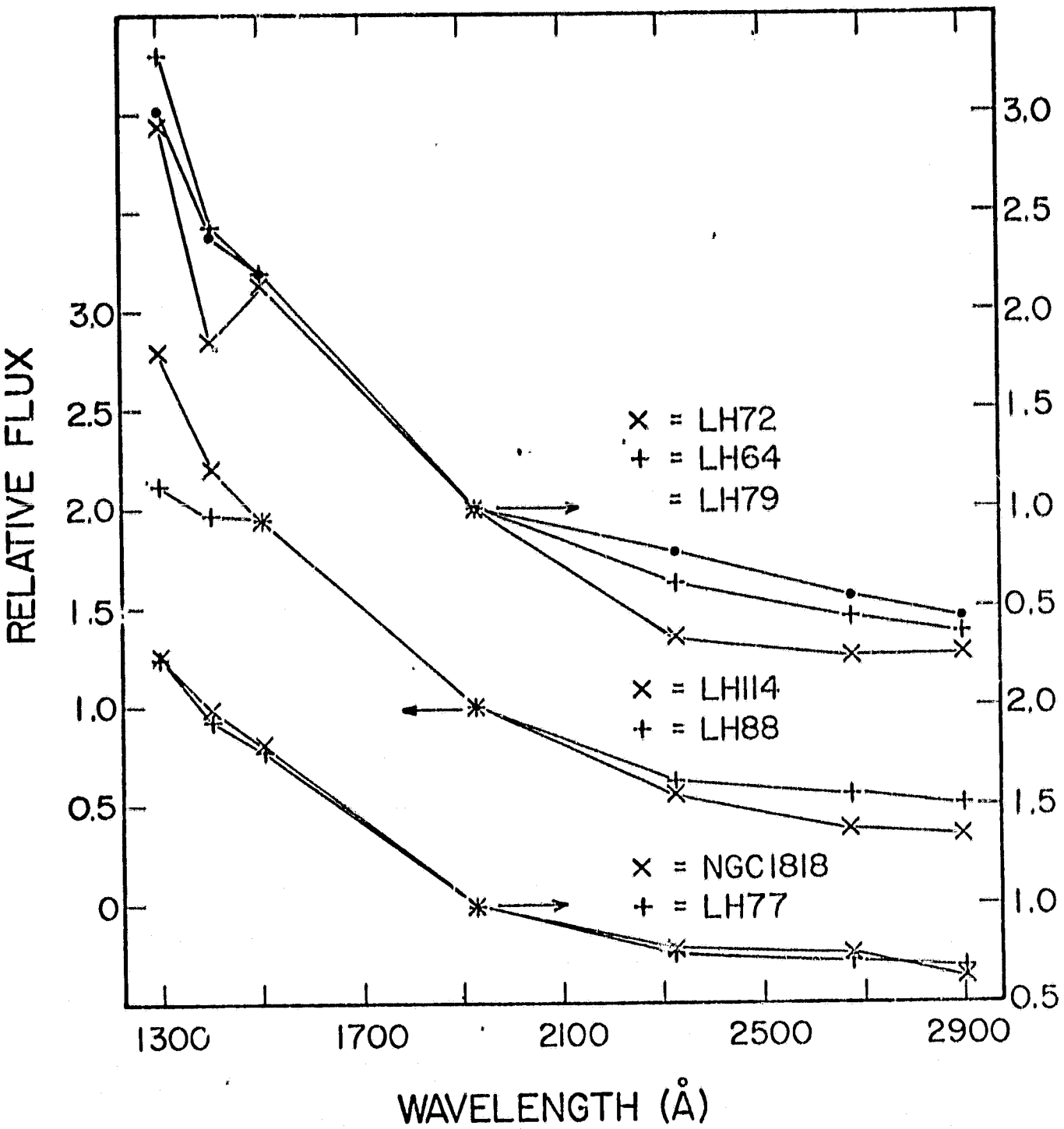
RELATIVE FLUX
WAVELENGTH (Å)
1300
1700
2100
2500
2900
3.0
2.5
2.0
1.5
1.0
0.5
0
× = LH72
+ = LH64
= LH79
× = LH114
+ = LH88
× = NGC1818
+ = LH77